*J. Fluid Mech.* (1988), *vol.* 190, *pp.* 531–559
*Printed in Great Britain*



# Stochastic estimation of organized turbulent structure: homogeneous shear flow

By RONALD J. ADRIAN† AND PARVIZ MOIN‡

† Department of Theoretical and Applied Mechanics, University of Illinois, Urbana, IL 61801, USA

‡ Department of Mechanical Engineering, Stanford University, Stanford CA 94305 USA *and* NASA Ames Research Center, Moffett Field, CA 94035, USA

(Received 23 February 1987)

The large-scale organized structures of turbulent flow can be characterized quantitatively by a conditional eddy, given the local kinematic state of the flow as specified by the conditional average of $\boldsymbol{u}(\boldsymbol{x}', t)$ given the velocity and the deformation tensor at a point $\boldsymbol{x}$: $\langle \boldsymbol{u}(\boldsymbol{x}', t) \,|\, \boldsymbol{u}(\boldsymbol{x}, t),\ \boldsymbol{d}(\boldsymbol{x}, t) \rangle$. By means of linear mean-square stochastic estimation, $\langle \boldsymbol{u}' \,|\, \boldsymbol{u}, \boldsymbol{d} \rangle$ is approximated in terms of the two-point spatial correlation tensor, and the conditional eddy is evaluated for arbitrary values of $\boldsymbol{u}(\boldsymbol{x}, t)$ and $\boldsymbol{d}(\boldsymbol{x}, t)$, permitting study of the turbulent field for a wide range of local kinematic states. The linear estimate is applied to homogeneous turbulent shear flow data generated by direct numerical simulation. The joint velocity–deformation probability density function is used to obtain conditions corresponding to those events that contribute most to the Reynolds shear stress. The primary contributions to the second-quadrant and fourth-quadrant Reynolds-stress events in homogeneous shear flow come from flow induced through the 'legs' and close to the 'heads' of upright and inverted 'hairpins', respectively.

The equation governing the joint probability density function of $f_{\boldsymbol{u},\boldsymbol{d}}(\boldsymbol{u}, \boldsymbol{d})$ is derived. It is shown that this equation contains $\langle \boldsymbol{u}' \,|\, \boldsymbol{u}, \boldsymbol{d} \rangle$ and that the equations for second-order closure can be derived from it. Closure requires approximation of $\langle \boldsymbol{u}' \,|\, \boldsymbol{u}, \boldsymbol{d} \rangle$.

## 1. Introduction

The investigation of large-scale organized structures requires methods capable of detecting the structures and determining quantitatively properties such as geometry, energy content and contribution to turbulent transport. Ideally, the methods should also provide a measure of the frequency of occurrence of the organized structure and information that can be incorporated into a turbulence model in a reasonably straightforward way. The development of techniques for this purpose is a recurrent topic in the literature (Willmarth 1978; Cantwell 1981; Hussain 1983). Generally, quantitative techniques such as spatial correlation do not describe the coherent structures in a readily interpretable manner, while qualitative techniques such as flow visualization reveal the structure (at sufficiently low Reynolds number), but they do not provide enough quantitative information. The characteristic-eddy method (Bakewell & Lumley 1967; Lumley 1970, 1981) combines Lumley's generalization of the Karhunen–Loevé expansion with a shot-noise model in which the flow field is decomposed into a set of randomly scattered deterministic eddies. It has been used recently to analyse flow structure in turbulent channel flow (Moin

1984). This approach is particularly useful when energy is concentrated in a few eigenmodes. However, the most common approach to coherent-structure analysis is the conditional-averaging method (Antonia 1981).

The general form of a conditional average is $\langle \boldsymbol{g}(\boldsymbol{u}) \,|\, \boldsymbol{E} \rangle$, where $\boldsymbol{E}$ is a conditional event vector, $\boldsymbol{g}$ is any function, and $\boldsymbol{u}' = \boldsymbol{u}(\boldsymbol{x}', t)$. The event $\boldsymbol{E}$ is usually viewed as a detector of coherent structure, but since the properties of coherent structures are not known *a priori*, it is difficult to define reliable, unambiguous and unbiased detector events. The VITA event (Blackwelder & Kaplan 1976) and the quadrant-analysis events (Willmarth & Lu 1974) are used widely for the detection of bursts and high-Reynolds-stress eddies. Each can be implemented using time-series measurements of one or two velocity components at a single point.

Recently, direct numerical simulations and large-eddy simulations of turbulence have been shown to be effective tools for the study of coherent structures in turbulent flows with geometrically simple boundaries (Moin & Kim 1985; Kim & Moin 1986). Conditional averages of the computed flows compare very favourably with experimental studies, indicating good simulation of the details of the turbulence structures. A unique feature of computational data bases is the availability of full vector-field data, making it feasible to use three-dimensional vector-based conditional events, rather than the scalar or two-dimensional events imposed upon most experimental studies. Existing work with conditional averages based upon vector events suggests that information contained in the vector appreciably enhances the capacity of the conditional average to delineate structure (Adrian 1978).

The conditional eddies defined in Adrian (1975, 1979) use an event

$$\boldsymbol{E}_{\boldsymbol{u}} = \boldsymbol{v} \leqslant \boldsymbol{u}(\boldsymbol{x}, t) < \boldsymbol{v} + \mathrm{d}\boldsymbol{v} \tag{1}$$

that confines the velocity vector $\boldsymbol{u}(\boldsymbol{x}, t)$ to a small window between $\boldsymbol{v}$ and $\boldsymbol{v}+\mathrm{d}\boldsymbol{v}$, where $\boldsymbol{v}$ is an arbitrary vector. The conditional average of $\boldsymbol{u}'$ is written variously as $\langle \boldsymbol{u}(\boldsymbol{x}', t) \,|\, \boldsymbol{u}(\boldsymbol{x}, t) \rangle$, $\langle \boldsymbol{u}(\boldsymbol{x}', t) \,|\, \boldsymbol{u}(\boldsymbol{x}, t) = \boldsymbol{v} \rangle$, $\langle \boldsymbol{u}(\boldsymbol{x}', t) \,|\, \boldsymbol{v} \rangle$ or $\langle \boldsymbol{u}(\boldsymbol{x}', t) \,|\, \boldsymbol{E}_{\boldsymbol{u}} \rangle$.

In isotropic turbulence, rotational and reflection invariance imply that $\langle \boldsymbol{u}' \,|\, \boldsymbol{u}(\boldsymbol{x}, t) \rangle$ must be a vector field axisymmetric around $\boldsymbol{u}(\boldsymbol{x}, t)$ (Adrian 1975). Estimates of this average using isotropic turbulence data reveal a vortex-ring structure whose axis of axisymmetry lies parallel to $\boldsymbol{u}(\boldsymbol{x}, t)$ (Adrian 1979; Tung & Adrian 1980). Specifying the complete three-dimensional vector renders the vortex ring observable by selecting from the ensemble of isotropically oriented vortex rings only those structures with a common alignment.

In flows whose random structures are less random than isotropic turbulence the conditional eddies can produce accurate maps of the coherent structures without specifying the complete three-dimensional vector. Studies using conditional events limited to two velocity components by Tung (1982) and Tung, Adrian & Jones (1987) in a plane shear layer, Hassan (1980) and Hassan, Jones & Adrian (1987) in turbulent pipe flow, and Chang, Adrian & Jones (1985) in the axisymmetric shear layer of a round jet each yielded conditional eddies that agreed closely with the coherent structures observed by other methods. Even so, it is likely that specification of the third velocity component would have made the flow patterns more specific.

The present paper deals with a generalization of the conditional-eddy concept in which the conditional event is extended to include a condition on the value of the deformation tensor

$$d_{ij}(\boldsymbol{x}, t) = \frac{\partial u_i}{\partial x_j}. \tag{2}$$

The conditional eddy becomes

$$\langle \boldsymbol{u}' \,|\, \boldsymbol{u}, \boldsymbol{d} \rangle = \langle \boldsymbol{u}(\boldsymbol{x}', t) \,|\, \boldsymbol{E}_{\boldsymbol{u},\boldsymbol{d}} \rangle, \tag{3}$$

where

$$\boldsymbol{E}_{\boldsymbol{u},\boldsymbol{d}} = \{\boldsymbol{v} \leqslant \boldsymbol{u}(\boldsymbol{x}, t) < \boldsymbol{v} + \mathrm{d}\boldsymbol{v}, \quad \boldsymbol{\Delta} \leqslant \boldsymbol{d}(\boldsymbol{x}, t) < \boldsymbol{\Delta} + \mathrm{d}\boldsymbol{\Delta}\}. \tag{4}$$

Concurrent investigations of conditional averages using this event in the context of isotropic turbulence show that the specification of $\boldsymbol{d}$ significantly modifies the conditional flow fields, especially when the given values of $\boldsymbol{u}(\boldsymbol{x}, t)$ are *weak* (Ditter 1987; J. L. Ditter & R. J. Adrian 1988, paper in preparation). A simple case in which the flow at $\boldsymbol{x}$ is dominated by the deformation tensor rather than the velocity occurs when $\boldsymbol{x}$ is a stagnation point of the velocity field.

The motivation for defining the generalized event $\boldsymbol{E}_{\boldsymbol{u},\boldsymbol{d}}$ derives from the elementary observation that the first-order kinematics at a point $\boldsymbol{x}$ are described by the local translation, as embodied in $\boldsymbol{u}(\boldsymbol{x}, t)$, and the rotation and the rate of strain, the latter two being contained in the deformation tensor. Thus, specifying only the velocity $\boldsymbol{u}(\boldsymbol{x}, t)$ renders an incomplete description of the kinematic state of the fluid at $(\boldsymbol{x}, t)$, corresponding to an average over all states of rotation and strain.

We shall refer to the average in (3) as a 'conditional eddy given the local kinematics', abbreviated to CELK. CELT eddies are defined as conditional eddies given the local translation, and CELD eddies are conditional on the local deformation. In all cases, of course, the conditional eddy is a deterministic vector function of $\boldsymbol{x}'$ in three spatial dimensions. As will be shown in §2 this vector function has many properties similar to the velocity vector, such as obeying the equation of continuity. The conditional eddy depends upon $\boldsymbol{u}(\boldsymbol{x}, t)$ and $\boldsymbol{d}(\boldsymbol{x}, t)$ parametrically. The statistical properties of CELK eddies and the probability-density-function equation governing their evolution will be presented in §2.

In §3 linear stochastic estimation will be applied to CELK eddies to find an approximation that can be evaluated for any combination of $\boldsymbol{u}$- and $\boldsymbol{d}$-values solely in terms of the two-point spatial correlation. This technique is a well-known procedure for estimating random variables (Papoulis 1984); its applicability to the estimation of conditional averages was first demonstrated by Adrian (1975, 1979) who applied it to conditional eddies given the velocities at one or more points. For isotropic turbulence the linear stochastic estimate given $\boldsymbol{E}_{\boldsymbol{u}}$ has the particularly simple form

$$\langle \boldsymbol{u}_i(\boldsymbol{x}+\boldsymbol{r}) \,|\, \boldsymbol{u}(\boldsymbol{x}) \rangle = R_{li}(\boldsymbol{r})\, u_l(\boldsymbol{x}) \langle u_1^2 \rangle$$

when $R_{li}$ is the two-point correlation tensor.

Linear stochastic approximation simplifies enormously the task of evaluating CELK eddies, and it makes feasible evaluation for many different values of $\boldsymbol{u}$ and $\boldsymbol{d}$ without performing different experiments. Indeed, it can be stated categorically that the evaluation of CELK eddies would not be possible without the implementation of stochastic estimation because the high dimensionality of the event $\boldsymbol{E}_{\boldsymbol{u},\boldsymbol{d}}$ makes it impossible, practically, to find a large number of realizations that satisfy the event. Thus, the primary results in this paper are those concerning stochastically estimated CELK eddies, rather than the CELK eddies *per se*. Our discussion of the CELK eddies in §2 is, however, a necessary precursor, as it lays the foundations for interpreting the stochastic estimates kinetically, dynamically and statistically.

In §4 linear stochastic estimation is applied to a numerical data base for homogeneous shear flow (Rogers & Moin 1987), and the propertes of the coherent hairpin vortex structures found from this procedure are discussed.

## 2. Conditional eddies given the local kinematics

### 2.1. *Properties*

In general, a conditional average is, in the least-mean-square error sense, the best nonlinear estimate of the quantity being averaged given the information contained in the event vector (Papoulis 1984). Specifically, the conditional average $\langle \boldsymbol{u}' \,|\, \boldsymbol{u}, \boldsymbol{d} \rangle$ is the best estimate of $\boldsymbol{u}(\boldsymbol{x}')$ given $\{\boldsymbol{u}(\boldsymbol{x}), \boldsymbol{d}(\boldsymbol{x})\}$ in the sense that the mean-square error

$$e_i = \langle [u_i' - \langle u_i' \,|\, \boldsymbol{u}, \boldsymbol{d} \rangle]^2 \rangle \tag{5}$$

is minimized for each component, $i = 1, 2, 3$. The average is over all possible values of the parameters $\boldsymbol{v}$ and $\boldsymbol{A}$ in the event $\boldsymbol{E}_{\boldsymbol{u},\boldsymbol{d}}$ (see (4)). It is convenient to perform the usual decomposition of $\boldsymbol{d}$ into a rate-of-strain tensor and a rotation tensor:

$$d_{ij} = e_{ij} + \xi_{ij}, \tag{6}$$

where

$$e_{ij} = \frac{1}{2}\left(\frac{\partial u_i}{\partial x_j} + \frac{\partial u_j}{\partial x_i}\right), \tag{7}$$

and

$$\xi_{ij} = \frac{1}{2}\left(\frac{\partial u_i}{\partial x_j} - \frac{\partial u_j}{\partial x_i}\right), \tag{8}$$

and the vorticity vector $\boldsymbol{\omega}$ is related to the rotation tensor by

$$\omega_i = \epsilon_{ijk}\, \xi_{jk}. \tag{9}$$

Then $\langle \boldsymbol{u}' \,|\, \boldsymbol{u}, \boldsymbol{d} \rangle$ is the best estimate of $\boldsymbol{u}(\boldsymbol{x}', t)$ given the complete kinematic state of the fluid at $\boldsymbol{x}$, as specified by the translation $\boldsymbol{u}$, the rotation $\boldsymbol{\omega}$, and the rate-of-strain $\boldsymbol{e}$.

One of the primary difficulties in the study of coherent structures is the lack of a mathematically precise definition of what, exactly, constitutes a coherent structure (Hussain 1983). This void lies at the root of the problem of defining proper detector events for conditional averages. In this regard, a substantial conceptual clarification is achieved if the conditional event is viewed not as detector, but solely as a statement of information about the flow at $\boldsymbol{x}$. Then, the conditional average does not *a priori* correspond to a coherent structure. If a correspondence does exist, it must be demonstrated by a separate and direct comparison of the conditional average with physical realizations that are deemed to be coherent structures on independent grounds.

To illustrate the logical necessity of distinguishing between a conditional average and the coherent structure, let us suppose that a flow field existed which possessed no structures that were judged to fit any of the prevailing definitions of a coherent structure. While coherent structure may not exist, it is certain for physically reasonable definitions of the event $\boldsymbol{E}$ that the conditional average would exist, showing that the coherent-structure concept is an independent entity. In fact, the conditional average $\langle \boldsymbol{u}' \,|\, \boldsymbol{E} \rangle$ will always define a non-zero vector function of $\boldsymbol{x}'$, provided only that the velocity $\boldsymbol{u}'$ and the conditional event $\boldsymbol{E}$ are statistically dependent. The possibility of statistical independence is precluded for conditional eddies based on the events $\boldsymbol{E}_{\boldsymbol{u}}$, or $\boldsymbol{E}_{\boldsymbol{u},\boldsymbol{d}}$ because, as $\boldsymbol{x}'$ approaches $\boldsymbol{x}$, $\boldsymbol{u}'$ approaches $\boldsymbol{u}$ and $\partial \boldsymbol{u}'/\partial \boldsymbol{x}'$ approaches $\boldsymbol{d}$, implying that $\boldsymbol{u}'$ can never be statistically independent of $\boldsymbol{E}_{\boldsymbol{u}}$ or $\boldsymbol{E}_{\boldsymbol{u},\boldsymbol{d}}$ for sufficiently small $|\boldsymbol{x}' - \boldsymbol{x}|$. Hence, *conditional eddy fields, given* $\boldsymbol{E}_{\boldsymbol{u},\boldsymbol{d}}$, *must exist for all turbulent flows in some neighbourhood of* $\boldsymbol{x}$. This property distinguishes

the events $\boldsymbol{E}_{\boldsymbol{u}}$ and $\boldsymbol{E}_{\boldsymbol{u},\boldsymbol{d}}$ from *ad hoc* events which may be highly correlated with the velocity in one type of flow, but only weakly correlated in another. (For example, the quadrant-detector event of Willmarth & Lu (1972) works well in shear flows, but it would have little success in flows with no Reynolds stress, such as free convection.)

Although the conceptual distinction between conditional eddies as mathematical entities and coherent structures as physical entities has been emphasized, it should not be inferred that conditional eddies cannot detect coherent structures. In fact, the conditional eddies are expected to correspond to the average physical structure very closely when the coherent structures are characterized by *unique* sets of values of $\boldsymbol{u}$ and/or $\boldsymbol{d}$ that are characteristic solely of that structure.

The CELK eddy has certain properties that follow from the coincidence, separation and reduction properties of the probability density functions for turbulence (Lundgren 1967; Papoulis 1984). They are as follows:

$$\lim_{\boldsymbol{x}'\to\boldsymbol{x}} \langle \boldsymbol{u}' \,|\, \boldsymbol{u}, \boldsymbol{d}\rangle = \boldsymbol{u}, \tag{10}$$

$$\lim_{|\boldsymbol{x}'-\boldsymbol{x}|\to\infty} \langle \boldsymbol{u}' \,|\, \boldsymbol{u}, \boldsymbol{d}\rangle = \langle \boldsymbol{u}'\rangle, \tag{11}$$

$$\langle\langle \boldsymbol{u}' \,|\, \boldsymbol{u}, \boldsymbol{d}\rangle\rangle = \langle \boldsymbol{u}'\rangle, \tag{12}$$

$$\langle\langle \boldsymbol{u}' \,|\, \boldsymbol{u}, \boldsymbol{d}\rangle \,|\, \boldsymbol{u}\rangle = \langle \boldsymbol{u}' \,|\, \boldsymbol{u}\rangle, \tag{13}$$

$$\langle\langle \boldsymbol{u}' \,|\, \boldsymbol{u}, \boldsymbol{d}\rangle \,|\, \boldsymbol{d}\rangle = \langle \boldsymbol{u}' \,|\, \boldsymbol{d}\rangle. \tag{14}$$

The coincidence property, equation (10), follows from the fact that $\boldsymbol{u}' \to \boldsymbol{u}$ as $\boldsymbol{x}' \to \boldsymbol{x}$, and $\boldsymbol{u}$ has a fixed value under the conditional-average operator. The separation property in (11) assumes that $\boldsymbol{u}'$ becomes statistically independent of $\boldsymbol{u}$ and $\boldsymbol{d}$ when $\boldsymbol{x}'$ is far removed from $\boldsymbol{x}$. The reduction properties in (12)–(14) follow from the definition of conditional probability (Papoulis 1984).

In (12), (13) and (14), it is convenient to interpret $\langle \boldsymbol{u}' \,|\, \boldsymbol{u}, \boldsymbol{d}\rangle$ as a deterministic function of the *random variables* $\boldsymbol{u}$ and $\boldsymbol{d}$. The outer average in (12) averages over all possible values of $\boldsymbol{u}$ and $\boldsymbol{d}$, resulting in the unconditional average of $\boldsymbol{u}'$. The conditional average in (13) averages over the set of realizations in which $\boldsymbol{u}$ is fixed, but $\boldsymbol{d}$ is not fixed, resulting in the conditional average of $\boldsymbol{u}'$ with $\boldsymbol{u}$ given.

The operations of conditional averaging and differentiation may be interchanged because they are linear. Then, the gradient of the conditional-eddy field is equal to the conditional average of the deformation tensor,

$$\frac{\partial}{\partial x_j'}\langle u_i' \,|\, \boldsymbol{u}, \boldsymbol{d}\rangle = \left\langle \frac{\partial u_i'}{\partial x_j'} \,\middle|\, \boldsymbol{u}, \boldsymbol{d} \right\rangle \tag{15a}$$

$$= \langle d_{ij}' \,|\, \boldsymbol{u}, \boldsymbol{d}\rangle. \tag{15b}$$

Since $d_{ii}' = 0$ for incompressible flow, (15*b*) shows that the conditional-eddy field for incompressible flow is solenoidal,

$$\frac{\partial}{\partial x_i'}\langle u_i' \,|\, \boldsymbol{u}, \boldsymbol{d}\rangle = 0. \tag{16}$$

This equation is analogous to Lundgren's (1967) divergence property. Similarly, it is apparent from (15*b*) that the vorticity and rate of strain of the conditional-eddy field are equal to the conditional averages of the vorticity and rate-of-strain of the turbulent field, respectively. From (15*b*), (10) and (11) it is easy to see that $\langle d_{ij} \,|\, \boldsymbol{u},$

$\boldsymbol{d}\rangle$ also possesses separation and coincidence properties, from which it can be inferred that the conditional vorticity approaches the given vorticity as $\boldsymbol{x}' \to \boldsymbol{x}$, and so on.

Finally, it must be noted that any unconditional moment involving the product of $\boldsymbol{u}'$ and/or its derivatives with any function $\boldsymbol{Q}(\boldsymbol{u}, \boldsymbol{d})$ can be obtained from the statistical information contained in $\langle \boldsymbol{u}' \,|\, \boldsymbol{u}, \boldsymbol{d}\rangle$ by averaging:

$$\langle \boldsymbol{Q}(\boldsymbol{u}, \boldsymbol{d}) \langle \boldsymbol{u}' \,|\, \boldsymbol{u}, \boldsymbol{d}\rangle\rangle = \langle\langle \boldsymbol{Q}(\boldsymbol{u}, \boldsymbol{d}) \boldsymbol{u}' \,|\, \boldsymbol{u}, \boldsymbol{d}\rangle\rangle \tag{17a}$$

$$= \langle \boldsymbol{Q}(\boldsymbol{u}, \boldsymbol{d}) \boldsymbol{u}'\rangle. \tag{17b}$$

Also,
$$\langle \boldsymbol{Q}(\boldsymbol{u}, \boldsymbol{d}) \langle \boldsymbol{d}' \,|\, \boldsymbol{u}, \boldsymbol{d}\rangle\rangle = \langle \boldsymbol{Q}(\boldsymbol{u}, \boldsymbol{d}) \boldsymbol{d}'\rangle. \tag{18}$$

By setting $\boldsymbol{Q}$ equal to $\boldsymbol{u}$ or $\boldsymbol{d}$, (17$b$) and (18) show that the CELK eddy contains the structure of the two-point spatial correlations between $\boldsymbol{u}$ and $\boldsymbol{u}'$, $\boldsymbol{u}$ and $\boldsymbol{d}'$, $\boldsymbol{u}'$ and $\boldsymbol{d}$, and $\boldsymbol{d}$ and $\boldsymbol{d}'$. While the structure of these correlations can in general be obtained exactly from $\langle \boldsymbol{u}' \,|\, \boldsymbol{u}, \boldsymbol{d}\rangle$ by averaging, the converse does not follow: it is not possible, in general, to obtain the conditional average exactly from the correlation functions. However, certain random processes do allow exact calculation of the conditional average from the correlation function. Joint normal processes are the best known example (Papoulis 1984). We shall also see that it is possible to *approximate* the conditional average in terms of the correlation functions.

### 2.2. *Probability density of the kinematic state*

Conditional averages must be considered in conjunction with the probability of the conditional event. The conditional average describes the spatial structure of the field, and the event probability describes the frequency with which the event occurs. The latter is *not* the same as the frequency with which the *structure* occurs, because a single coherent structure may have many events, both similar and different, associated with its field. Thus, a hairpin vortex has vorticity pointing in one direction on one leg, but in the opposite direction on the other, and either condition is a legitimate event characterizing the spatial structure of the hairpin.

The natural combination of the conditional eddy and the probability density is contained in the equation for the one-point probability density

$$f_{\boldsymbol{u}}(\boldsymbol{v}, \boldsymbol{x}, t)\,\mathrm{d}\boldsymbol{v} = \mathrm{Prob}\{\boldsymbol{v} \leqslant \boldsymbol{u}(\boldsymbol{x}, t) < \boldsymbol{v} + \mathrm{d}\boldsymbol{v}\}], \tag{19}$$

wherein the conditional averages $\langle \boldsymbol{u}' \,|\, \boldsymbol{u}\rangle$ and $\langle \boldsymbol{u}'\boldsymbol{u}' \,|\, \boldsymbol{u}\rangle$ always appear multiplied by $f_{\boldsymbol{u}}$ (Adrian 1975):†

$$\frac{\partial f_{\boldsymbol{u}}}{\partial t} + v_j \frac{\partial f_{\boldsymbol{u}}}{\partial x_j} = -\frac{\partial}{\partial v_k}\left\{ f_{\boldsymbol{u}} \left[ -\frac{1}{4\pi} \int_{\boldsymbol{x}'} \left( \frac{\partial}{\partial x_k} \frac{1}{|\boldsymbol{x} - \boldsymbol{x}'|} \right) \left( \frac{\partial}{\partial x_i'} \frac{\partial}{\partial x_j'} \right) \langle u_i' u_j' \,|\, \boldsymbol{v}\rangle \,\mathrm{d}^3\boldsymbol{x}' \right.\right.$$
$$\left.\left. + \lim_{\boldsymbol{x}' \to \boldsymbol{x}} \nu \frac{\partial}{\partial x_i'} \frac{\partial}{\partial x_i'} \langle u_k' \,|\, \boldsymbol{v}\rangle \right] \right\}. \tag{20}$$

(This equation was derived from Lundgren's (1967) original equation by recasting the terms involving the two-point probability density function into two-point conditional averages.) One sees conditional averages occurring in the viscous term and in the term representing the pressure. The commutivity of the operations of

† We shall use the notation $\langle \boldsymbol{u}' \,|\, \boldsymbol{E}_{\boldsymbol{u}}\rangle$, $\langle \boldsymbol{u}' \,|\, \boldsymbol{v}\rangle$ and $\langle \boldsymbol{u}' \,|\, \boldsymbol{u}\rangle$ interchangeably, and likewise for $\langle \boldsymbol{u}' \,|\, \boldsymbol{u}, \boldsymbol{d}\rangle$, $\langle \boldsymbol{u}' \,|\, \boldsymbol{E}_{\boldsymbol{u},\boldsymbol{d}}\rangle$ and $\langle \boldsymbol{u}' \,|\, \boldsymbol{v}, \boldsymbol{\Delta}\rangle$.

differentiation and ensemble averaging implies that the derivative of the conditional average $\langle \boldsymbol{u}' \,|\, \boldsymbol{v} \rangle$ in the viscous term equals the conditional average of the derivative. Hence, the entire term represents the best mean-square estimate of the net viscous force per unit mass given that the velocity of the fluid has the value $\boldsymbol{v}$ at the point $\boldsymbol{x}$. Likewise, the pressure term represents the conditionally averaged pressure force per unit mass given that the velocity is $\boldsymbol{v}$ at $\boldsymbol{x}$. The conditional average $\langle \boldsymbol{u}'\boldsymbol{u}' \,|\, \boldsymbol{v} \rangle$ is the best mean-square estimate of the Reynolds stress at $\boldsymbol{x}'$.

Equation (20) demonstrates the clear link between conditional eddies and the closure problem for turbulence, and it provides a straightforward method of interpreting the dynamical implications of conditional-eddy structure.

In this section we shall derive for incompressible, constant-property turbulent flow the equation governing the probability density function for $\boldsymbol{u}$ and $\boldsymbol{d}$, as defined by

$$f_{\boldsymbol{u},\boldsymbol{d}}(\boldsymbol{v}, \boldsymbol{\Delta}; \boldsymbol{x}, t)\,\mathrm{d}\boldsymbol{v}\,\mathrm{d}\boldsymbol{\Delta} = \mathrm{Prob}\{\boldsymbol{v} \leqslant \boldsymbol{u}(\boldsymbol{x}, t) < \boldsymbol{v} + \mathrm{d}\boldsymbol{v}, \quad \boldsymbol{\Delta} \leqslant \boldsymbol{d}(\boldsymbol{x}, t) < \boldsymbol{\Delta} + \mathrm{d}\boldsymbol{\Delta}\}. \tag{21}$$

Following Lundgren (1967) the derivation begins with the identity

$$\langle \delta(\boldsymbol{u}(\boldsymbol{x}, t) - \boldsymbol{v})\,\delta(\boldsymbol{d}(\boldsymbol{x}, t) - \boldsymbol{\Delta}) \rangle \equiv \int \delta(\boldsymbol{u} - \boldsymbol{v})\,\delta(\boldsymbol{d} - \boldsymbol{\Delta}) f_{\boldsymbol{u},\boldsymbol{d}}(\boldsymbol{u}, \boldsymbol{d}; \boldsymbol{x}, t)\,\mathrm{d}\boldsymbol{u}\,\mathrm{d}\boldsymbol{d} \tag{22a}$$

$$= f_{\boldsymbol{u},\boldsymbol{d}}(\boldsymbol{v}, \boldsymbol{\Delta}; \boldsymbol{x}, t). \tag{22b}$$

The time derivative of $f_{\boldsymbol{u},\boldsymbol{d}}$ is calculated from (22$b$):

$$\dot{f}_{\boldsymbol{u},\boldsymbol{d}} = \langle \dot{\delta}(\boldsymbol{u} - \boldsymbol{v})\,\delta(\boldsymbol{d} - \boldsymbol{\Delta}) + \delta(\boldsymbol{u} - \boldsymbol{v})\,\dot{\delta}(\boldsymbol{d} - \boldsymbol{\Delta}) \rangle \tag{23a}$$

$$= \left\langle \dot{u}_i \left[ \frac{\partial \delta(\boldsymbol{u} - \boldsymbol{v})}{\partial u_i} \right] \delta(\boldsymbol{d} - \boldsymbol{\Delta}) + \delta(\boldsymbol{u} - \boldsymbol{v})\,\dot{d}_{ij} \left[ \frac{\partial \delta(\boldsymbol{d} - \boldsymbol{\Delta})}{\partial d_{ij}} \right] \right\rangle \tag{23b}$$

$$= -\frac{\partial}{\partial v_i} \langle \dot{u}_i\,\delta(\boldsymbol{u} - \boldsymbol{v})\,\delta(\boldsymbol{d} - \boldsymbol{\Delta}) \rangle - \frac{\partial}{\partial \Delta_{ij}} \langle \dot{d}_{ij}\,\delta(\boldsymbol{u} - \boldsymbol{v})\,\delta(\boldsymbol{d} - \boldsymbol{\Delta}) \rangle \tag{23c}$$

$$= -\frac{\partial}{\partial v_i} \{ \langle \dot{u}_i \,|\, \boldsymbol{v}, \boldsymbol{\Delta} \rangle f_{\boldsymbol{u},\boldsymbol{d}}(\boldsymbol{v}, \boldsymbol{\Delta}) \} - \frac{\partial}{\partial \Delta_{ij}} \{ \langle \dot{d}_{ij} \,|\, \boldsymbol{v}, \boldsymbol{\Delta} \rangle f_{\boldsymbol{u},\boldsymbol{d}}(\boldsymbol{v}, \boldsymbol{\Delta}) \}. \tag{23d}$$

Equations (23$a$–$c$) are obtained by obvious manipulations. Equation (23$d$) uses the relation

$$\langle \dot{\boldsymbol{u}}\delta(\boldsymbol{u} - \boldsymbol{v})\,\delta(\boldsymbol{d} - \boldsymbol{\Delta}) \rangle = \int \dot{\boldsymbol{u}}\delta(\boldsymbol{u} - \boldsymbol{v})\,\delta(\boldsymbol{d} - \boldsymbol{\Delta}) f_{\dot{\boldsymbol{u}},\boldsymbol{u},\boldsymbol{d}}(\dot{\boldsymbol{u}}, \boldsymbol{u}, \boldsymbol{d}; \boldsymbol{x}, t)\,\mathrm{d}\dot{\boldsymbol{u}}\,\mathrm{d}\boldsymbol{u}\,\mathrm{d}\boldsymbol{d} \tag{24a}$$

$$= \int \dot{\boldsymbol{u}} f_{\dot{\boldsymbol{u}},\boldsymbol{u},\boldsymbol{d}}(\dot{\boldsymbol{u}}, \boldsymbol{v}, \boldsymbol{\Delta}; \boldsymbol{x}, t)\,\mathrm{d}\dot{\boldsymbol{u}} \tag{24b}$$

$$= \int \dot{\boldsymbol{u}} f(\dot{\boldsymbol{u}} \,|\, \boldsymbol{v}, \boldsymbol{\Delta}) f_{\boldsymbol{u},\boldsymbol{d}}(\boldsymbol{v}, \boldsymbol{\Delta}; \boldsymbol{x}, t)\,\mathrm{d}\dot{\boldsymbol{u}} \tag{24c}$$

$$= \langle \dot{\boldsymbol{u}} \,|\, \boldsymbol{v}, \boldsymbol{\Delta} \rangle f_{\boldsymbol{u},\boldsymbol{d}}(\boldsymbol{v}, \boldsymbol{\Delta}; \boldsymbol{x}, t), \tag{24d}$$

wherein $f(\dot{\boldsymbol{u}} \,|\, \boldsymbol{v}, \boldsymbol{\Delta})$ is the conditional probability density of $\dot{\boldsymbol{u}}$ given $\boldsymbol{u} = \boldsymbol{v}$ and $\boldsymbol{d} = \boldsymbol{\Delta}$, defined by

$$f(\dot{\boldsymbol{u}} \,|\, \boldsymbol{v}, \boldsymbol{\Delta}) \equiv f_{\dot{\boldsymbol{u}},\boldsymbol{u},\boldsymbol{d}}(\dot{\boldsymbol{u}}, \boldsymbol{v}, \boldsymbol{\Delta}; \boldsymbol{x}, t) / f_{\boldsymbol{u},\boldsymbol{d}}(\boldsymbol{v}, \boldsymbol{\Delta}; \boldsymbol{x}, t). \tag{25}$$

The conditional average is found from the conditional density,

$$\langle \dot{\boldsymbol{u}} \,|\, \boldsymbol{v}, \boldsymbol{\Delta} \rangle \equiv \int \dot{\boldsymbol{u}} f(\dot{\boldsymbol{u}} \,|\, \boldsymbol{v}, \boldsymbol{\Delta}) \, \mathrm{d}\dot{\boldsymbol{u}}. \tag{26}$$

A relationship similar to (24$d$) is also used for $\langle \dot{d}_{ij} \delta(\boldsymbol{u}-\boldsymbol{v}) \delta(\boldsymbol{d}-\boldsymbol{\Delta}) \rangle$.

The rates of temporal evolution of $\boldsymbol{u}$ and $\boldsymbol{d}$ are governed by the incompressible, constant-property Navier–Stokes equation

$$\dot{u}_i = -u_k d_{ik} - \frac{1}{\rho}\frac{\partial p}{\partial x_i} + \nu \frac{\partial d_{ik}}{\partial x_k}, \tag{27}$$

the continuity equation

$$d_{ii} = 0, \tag{28}$$

and the derivative of (27)

$$\dot{d}_{ij} = -u_k \frac{\partial d_{ij}}{\partial x_k} - d_{kj} d_{ik} - \frac{1}{\rho}\frac{\partial^2 p}{\partial x_i \partial x_j} + \nu \frac{\partial^2 d_{ij}}{\partial x_k \partial x_k}, \tag{29}$$

where the pressure may be written as

$$p = -\frac{\rho}{4\pi} \int \frac{1}{|\boldsymbol{x}'-\boldsymbol{x}|} d'_{lm} d'_{ml} \, \mathrm{d}\boldsymbol{x}' \tag{30}$$

in an unbounded turbulent flow. The conditionally averaged values of $\dot{u}_i$ and $\dot{d}_{ij}$, obtained by averaging equations (27) and (29), are

$$\langle \dot{u}_i \,|\, \boldsymbol{v}, \boldsymbol{\Delta} \rangle = -v_k \Delta_{ik} + \frac{\partial}{\partial x_i}\left\{ \frac{1}{4\pi} \int \frac{1}{|\boldsymbol{x}'-\boldsymbol{x}|} \langle d'_{lm} d'_{lm} \,|\, \boldsymbol{v}, \boldsymbol{\Delta} \rangle \, \mathrm{d}\boldsymbol{x}' \right\} + \nu \lim_{\boldsymbol{x}' \to \boldsymbol{x}} \frac{\partial}{\partial x'_k} \langle d'_{ik} \,|\, \boldsymbol{v}, \boldsymbol{\Delta} \rangle \tag{31}$$

$$\langle \dot{d}_{ij} \,|\, \boldsymbol{v}, \boldsymbol{\Delta} \rangle = -v_k \lim_{\boldsymbol{x}' \to \boldsymbol{x}} \frac{\partial}{\partial x'_k} \langle d'_{ij} \,|\, \boldsymbol{v}, \boldsymbol{\Delta} \rangle - \Delta_{kj} \Delta_{ik} + \frac{\partial^2}{\partial x_i \partial x_j}\left\{ \frac{1}{4\pi} \int \frac{1}{|\boldsymbol{x}'-\boldsymbol{x}|} \langle d'_{lm} d'_{ml} \,|\, \boldsymbol{v}, \boldsymbol{\Delta} \rangle \, \mathrm{d}\boldsymbol{x} \right\} + \nu \lim_{\boldsymbol{x}' \to \boldsymbol{x}} \frac{\partial^2}{\partial x'_k \partial x'_k} \langle d'_{ij} \,|\, \boldsymbol{v}, \boldsymbol{\Delta} \rangle. \tag{32}$$

Equation (23$d$) plus (31) and (32) constitute the complete equation for $f_{\boldsymbol{u},\boldsymbol{d}}$. The conditional acceleration $\langle \dot{\boldsymbol{u}} \,|\, \boldsymbol{v}, \boldsymbol{\Delta} \rangle$ depends upon the conditional viscous stress and the conditional pressure stress. The stresses have been expressed in terms of $\langle \boldsymbol{d}' \,|\, \boldsymbol{v}, \boldsymbol{\Delta} \rangle$ and $\langle \boldsymbol{d}'\boldsymbol{d}' \,|\, \boldsymbol{v}, \boldsymbol{\Delta} \rangle$ which, in turn, can be written in terms of the conditional eddy, given the local kinematics,

$$\langle d'_{ij} \,|\, \boldsymbol{v}, \boldsymbol{\Delta} \rangle = \frac{\partial}{\partial x'_j} \langle u'_i \,|\, \boldsymbol{v}, \boldsymbol{\Delta} \rangle, \tag{33}$$

and the kinematically specified conditional Reynolds stress

$$\langle d'_{lm} d'_{ml} \,|\, \boldsymbol{v}, \boldsymbol{\Delta} \rangle = \frac{\partial^2}{\partial x'_m \partial x'_l} \langle u'_l u'_m \,|\, \boldsymbol{v}, \boldsymbol{\Delta} \rangle. \tag{34}$$

These conditional averages cannot be calculated from $f_{\boldsymbol{u},\boldsymbol{d}}$, and they constitute the essential closure problem for the $f_{\boldsymbol{u},\boldsymbol{d}}$ equation. (Conditional Reynolds stresses of the form $\langle u'_l u'_m \,|\, \boldsymbol{v} \rangle$ have been measured by Tung 1982.)

The differential equations for any statistical moment involving $\boldsymbol{u}$ or $\boldsymbol{d}$ can be

derived from the equation for $f_{u,d}$ by multiplying by the appropriate quantity and integrating, as in Lundgren (1967). In particular, the evolution equations for the mean flow, the Reynolds-stress tensor, the turbulent viscous dissipation, and the mean-square vorticity can each be derived directly from the equation for $f_{u,d}$. These moment equations encompass all current second-order closure models of turbulence.

Closure of the equation for $f_{u,d}$ requires approximation of $\langle \boldsymbol{u}' \,|\, \boldsymbol{u}, \boldsymbol{d} \rangle$ and $\langle \boldsymbol{u}'\boldsymbol{u}' \,|\, \boldsymbol{u}, \boldsymbol{d} \rangle$ in terms of $f_{u,d}$ or lower-order moments derivable from it. Since the equations governing the single-point moments that are the variables in all second-order closure models (kinetic energy, Reynolds stress, dissipation, mean-square vorticity, etc.) can be derived from the equation for $f_{u,d}$, but cannot be derived from any simpler probability density, it follows that the problem of *second-order closure* ultimately reduces to the approximation of $\langle \boldsymbol{u}' \,|\, \boldsymbol{u}, \boldsymbol{d} \rangle$ and $\langle \boldsymbol{u}'\boldsymbol{u}' \,|\, \boldsymbol{u}, \boldsymbol{d} \rangle$. That is, the unclosed terms in the moment equations would be closed by approximations to $\langle \boldsymbol{u}' \,|\, \boldsymbol{u}, \boldsymbol{d} \rangle$ and $\langle \boldsymbol{u}'\boldsymbol{u}' \,|\, \boldsymbol{u}, \boldsymbol{d} \rangle$ which would close the probability-density-function equation. Thus, *all closures of second-order moment equations implicitly involve approximations of the CELK eddies and their Reynolds-stress counterparts.*

Since the deformation tensor $\boldsymbol{d}(\boldsymbol{x})$ can always be obtained from the velocities at two points by taking the limit of $(\boldsymbol{u}_2 - \boldsymbol{u}_1)/(\boldsymbol{x}_2 - \boldsymbol{x}_1)$ as $\boldsymbol{x}_1$ and $\boldsymbol{x}_2$ approach $\boldsymbol{x}$, it is clear that the CELK event $\{\boldsymbol{u}, \boldsymbol{d}\}$ is a subset of the general two-point velocity event $\{\boldsymbol{u}_1, \boldsymbol{u}_2\}$, where $\boldsymbol{u}_1$ and $\boldsymbol{u}_2$ are evaluated at *arbitrary* points $\boldsymbol{x}_1$ and $\boldsymbol{x}_2$. In terms of the closure problem for the Lundgren–Monin p.d.f. hierarchy, we may think of $\{\boldsymbol{u}, \boldsymbol{d}\}$ as a *one-and-one-half point* event which defines a p.d.f. $f_{u,d}$ whose information content lies between that of the one-point p.d.f. and that of the full two-point p.d.f. Closure of the p.d.f. hierarchy at the one-and-one-half point level may be a useful approach to turbulence modelling in that it eliminates two-point information that is not needed for generalized second-order-moment models.

The CELK eddies play the role of supplying the information about the spatial structure of the turbulent flow. This information is sufficient to close the equations, and it is precisely the type of information that has been sought in the study of coherent structures. Hence, CELK eddies provide a means of incorporating phenomenological coherent-structure information into a statistical theory of turbulent transport.

## 3. Linear estimation of conditional eddies

Direct calculation of conditional eddies from experimental or numerical data is made difficult by the relatively high dimension of the conditional events, $N = 3$ in the case of $\boldsymbol{E}_u$ and $N = 12$ in the case of $\boldsymbol{E}_{ud}$. The high dimension has two ramifications. First, the probability of an event cell in the space of all events becomes small when $N$ is large. If the probability of a one-dimensional event is of order $P_0$, the probability of the multidimensional event is of order $P_0^N$. Thus, when the event windows $\mathrm{d}\boldsymbol{v}$ or $\mathrm{d}\boldsymbol{\Delta}$ are made small for the sake of highly specific conditioning, the value of $P_0^N$ becomes extremely small for CELT eddies and intolerably small for CELK eddies. To generate a number of samples sufficient to yield statistically stable estimates of the conditional averages, the data base must be correspondingly huge. For example, if $10^4$ samples satisfying the conditional event are needed for averaging and $P_0 = 0.1$, the total number of samples is of order $10^7$ for one conditional event of a CELT eddy, and of order $10^{16}$ for a CELK eddy. Computation of CELT eddies is feasible with current data bases, but direct computation of CELK eddies is clearly beyond existing capabilities.

The second consequence of high dimensionality is the difficulty which arises in selecting a particular conditional event from the large space of possible events. This is a natural consequence of using a highly specific type of event, and it means that the CELK eddy might have to be evaluated at a very large number of points in the event space to achieve an unbiased picture of the flow structure.

The sampling problem can be surmounted by application of linear stochastic estimation methods to the conditional average (Adrian 1975, 1979). The linear estimate permits evaluation of the conditional average for *any* value of the conditional-event vector in terms of simple correlation functions without recourse to conditionally sampling the data. The event selection problem is addressed effectively by combining linear estimation with the probability density function of the events. This allows determination of the frequency of occurrence of a structure as well as its contribution to various turbulence statistics (e.g. Reynolds shear stress or kinetic energy).

### 3.1. *Estimation procedure*

In linear stochastic estimation, the conditional average is approximated by a linear function of the given data, and the coefficients of the approximation depend upon second-order correlations between the data and the variable to be estimated. Nonlinear estimation retains higher-order terms in the approximate expansion of the conditional average, and the coefficients depend upon higher-order correlations (Tung & Adrian 1980). Linear estimates of $\langle \boldsymbol{u}' \,|\, \boldsymbol{u} \rangle$ predict that the conditional eddies of isotropic turbulence are vortex rings centred on $\boldsymbol{u}(\boldsymbol{x}, t)$ (Adrian 1978, 1979). Linear estimates of the structure of turbulent pipe flow by Hassan (1980) and Hassan *et al.* (1987) predict large eddies with azimuthal vorticity. Nithianandan's (1980) and Nithianandan, Jones & Adrian's (1987) linear estimates of the conditional average of two-dimensional velocity given the pressure fluctuations $\langle \boldsymbol{u}(\boldsymbol{x}', t) \,|\, p(\boldsymbol{x}, t) \rangle$ in an axisymmetric shear layer indicate the usual shear-layer pattern of transverse vortices, as do Tung's (1982) and Tung *et al.*'s (1987) estimates of $\langle \boldsymbol{u}(\boldsymbol{x}', t) \,|\, \boldsymbol{u}(\boldsymbol{x}, t) \rangle$ in a high-Reynolds-number plane turbulent shear layer. Linear estimates of the conditional pressure field $\langle p(\boldsymbol{x}', t) \,|\, \boldsymbol{u}(\boldsymbol{x}, t) \rangle$ in an axisymmetric shear layer performed by Chang *et al.* (1985) show regions of low pressure in the vortex cores separated by regions of high pressure in the stagnation-point flows on the braids separating the cores.

Extensive comparisons of measured conditional averages and their linear estimates in each of the aforementioned studies indicate that the estimates describe the large-scale structure of the conditional eddy with good accuracy. Evaluations of the contributions of higher-order terms in non-linear estimates show that the accuracy of the linear estimate is due to the relatively small magnitude of the higher-order terms for *probable* values of the data (Tung & Adrian 1980; Hassan 1980; Hassan *et al.* 1987). That is, the large values of the data that are needed to create significant nonlinear effects occur with low probability.

When estimating the conditional average, it is convenient to note that specifying the value of a *fluctuation at* $\boldsymbol{x}$ is statistically equivalent to specifying the value of the *total* quantity, since the mean value is a non-random number. Also, estimating the conditional average of the total is equivalent to estimating the conditional average of the fluctuation, since the mean can always be added to the conditional fluctuation. The estimation equations, especially those for nonlinear estimates, simplify considerably when conditional averages of fluctuations are estimated in terms of

fluctuating data. Hence, throughout this section $\boldsymbol{u}$ and $\boldsymbol{d}$ will represent zero mean fluctuations unless otherwise stated. We will also suppress the time dependence in the arguments of our variables since all variables will be evaluated at the same points in time. (Space–time conditional averages and their mean-square stochastic estimates are obvious generalizations that will not be considered here.)

The CELK eddy is a function of the data $\boldsymbol{u}(\boldsymbol{x})$ and $\boldsymbol{d}(\boldsymbol{x})$. It is approximated by expanding $\langle \boldsymbol{u}' \,|\, \boldsymbol{u}, \boldsymbol{d} \rangle$ in a Taylor series about the state $\boldsymbol{u} = 0$ and $\boldsymbol{d} = 0$. The constant term in the expansion vanishes because we are approximating a zero mean fluctuation. Neglecting terms of order two and higher yields the *linear estimate* of $\langle u_i' \,|\, \boldsymbol{u}, \boldsymbol{d} \rangle$

$$\hat{u}_i' = A_{ij}(\boldsymbol{x}', \boldsymbol{x})\, u_j(\boldsymbol{x}) + B_{ijk}(\boldsymbol{x}', \boldsymbol{x})\, d_{jk}(\boldsymbol{x}), \quad i, j, k = 1, 2, 3, \text{ excluding } j = k = 3. \tag{35}$$

The estimate excludes $d_{33}$ because it depends linearly on $d_{11}$ and $d_{22}$ through the continuity equation. (It can be shown that the use of linearly dependent data leads to non-uniqueness in the solutions for $\boldsymbol{A}$ and $\boldsymbol{B}$, although the estimate continues to be unique.

The estimation coefficients from the Taylor series expansion are unknown, and must be determined by another means. They are found by minimizing the mean-square error

$$e_i = \langle (\langle u_i' \,|\, \boldsymbol{u}, \boldsymbol{d} \rangle - \hat{u}_i')^2 \rangle \tag{36}$$

for $i = 1, 2, 3$. Note that $e_i$ is the error averaged over all possible states of the conditional event. Minimization of $e_i$ requires

$$\frac{\partial e_i}{\partial A_{il}} = 0, \quad \frac{\partial e_i}{\partial B_{ilm}} = 0, \qquad \begin{matrix} i, l, m = 1, 2, 3 \text{ except } l = m = 3 \\ \text{(no summation } i\text{)} \end{matrix}. \tag{37}$$

Differentiating (36) according to (35) and (37) yields

$$\langle (\langle u_i' \,|\, \boldsymbol{u}, \boldsymbol{d} \rangle - \hat{u}_i')\, u_l \rangle = 0, \quad i, l = 1, 2, 3 \tag{38a}$$

and

$$\langle (\langle u_i' \,|\, \boldsymbol{u}, \boldsymbol{d} \rangle - \hat{u}_i')\, d_{lm} \rangle = 0, \quad i, l, m = 1, 2, 3 \text{ except } l = m = 3, \tag{38b}$$

showing that error must be statistically orthogonal to each of the data. This *Orthogonality Principle* is used widely in linear estimation (Papoulis 1984), and it is readily generalized to nonlinear estimation.

Substituting (35) into (38), carrying out the indicated averaging operation and rearranging yields three sets ($i = 1, 2, 3$) of eleven linear algebraic equations for the thirty-three independent coefficients contained in $A_{ij}$ and $B_{ijk}$:

$$\left.\begin{aligned} A_{ij}\langle u_j u_l \rangle + B_{ijk}\langle d_{jk} u_l \rangle &= \langle u_l u_i' \rangle, \\ A_{ij}\langle u_j d_{lm} \rangle + B_{ijk}\langle d_{jk} d_{lm} \rangle &= \langle d_{lm} u_i' \rangle, \end{aligned}\right\} \quad \begin{matrix} i, j, k, l, m = 1, 2, 3 \\ \text{except } l = m = 3, j = k = 3. \end{matrix} \tag{39a, b}$$

These equations pertain, in general, to inhomogeneous, incompressible turbulence. The correlations in the left-hand side of (39) are single-point correlations at $\boldsymbol{x}$, and those on the right-hand side are two-point correlations computed at $\boldsymbol{x}$ and $\boldsymbol{x}'$.

### 3.2. *Properties of the linear estimate*

The linear estimate of the conditional average defined by (35) and (39) satisfies many of the same properties as the conditional average itself. Specifically, if $\boldsymbol{u}'$ and $\boldsymbol{u}$ each

have zero mean value (implying that $\boldsymbol{d}'$ and $\boldsymbol{d}$ are also zero-mean random variables), then

$$\lim_{x'\to x} \hat{u}'_i = u_i(\boldsymbol{x}), \quad \lim_{x'\to x} \frac{\partial \hat{u}'_i}{\partial x'_j} = d_{ij}(\boldsymbol{x}), \quad \lim_{|x'-x|\to\infty} \hat{u}'_i = 0; \tag{40a, b, c}$$

$$\langle \hat{u}'_i \rangle = 0, \tag{41}$$

$$\langle \hat{u}'_i \,|\, \boldsymbol{u} \rangle = A_{ij} u_j + B_{ijk} \langle d_{jk} \,|\, \boldsymbol{u} \rangle, \tag{42}$$

$$\langle \hat{u}'_i \,|\, \boldsymbol{d} \rangle = A_{ij} \langle u_j \,|\, \boldsymbol{d} \rangle + B_{ijk} d_{jk}, \tag{43}$$

$$\frac{\partial \hat{u}'_i}{\partial x'_j} = \langle d'_{ij} \,|\, \boldsymbol{u}, \boldsymbol{d} \rangle = \hat{d}'_{ij}, \tag{44}$$

$$\frac{\partial \hat{u}'_i}{\partial x'_i} = 0, \tag{45}$$

$$\langle u_l \hat{u}'_i \rangle = \langle u_l u'_i \rangle, \quad \langle d_{lm} \hat{u}'_i \rangle = \langle d_{lm} u'_i \rangle, \tag{46a, b}$$

$$\langle d_{lm} \hat{d}'_{ik} \rangle = \langle d_{lm} d'_{ik} \rangle, \quad \langle u_l \hat{d}'_{ik} \rangle = \langle u_l d'_{ik} \rangle. \tag{46c, d}$$

The coincidence properties in (40$a$, $b$) follow from the orthogonality principle and the fact that the conditional data contain the quantities being averaged. The separation property in (40$c$) follows immediately from the form of the solutions for $\boldsymbol{A}$ and $\boldsymbol{B}$ and the assumption that the two-point correlations in (39$a$, $b$) vanish for $|\boldsymbol{x}'-\boldsymbol{x}| \to \infty$. The reduction properties in (41), (42) and (43) result from directly averaging (35). Equation (44) states that the deformation tensor of the linear estimate is equal to the linear estimate of the deformation tensor. It can be shown by direct calculation of the quantities on each side. As a consequence, the deformation field of the linear estimate $d'_{ij}$ has properties that parallel those of the deformation field of the conditional average. The coincidence property in (40$b$) is one of these, and $\hat{d}'_{ij}$ also satisfies a separation property analogous to (40$c$). The divergence property in (45) follows from (44) and the assumption of incompressibility.

Equations (46$a$–$d$) state that moments involving the estimates $\hat{\boldsymbol{u}}'$ and $\hat{\boldsymbol{d}}'$ and first-order powers of $\boldsymbol{u}$ and $\boldsymbol{d}$ result *exactly* in the corresponding moments involving $\langle \boldsymbol{u}' \,|\, \boldsymbol{u}, \boldsymbol{d} \rangle$, $\langle \boldsymbol{d}' \,|\, \boldsymbol{u}, \boldsymbol{d} \rangle$ and first powers of $\boldsymbol{u}$ or $\boldsymbol{d}$. The equations correspond to (17) and (18) for $\boldsymbol{Q} = \boldsymbol{u}$ or $\boldsymbol{Q} = \boldsymbol{d}$. The linear estimate cannot guarantee that moments involving $\hat{\boldsymbol{u}}'$ or $\hat{\boldsymbol{d}}'$ and *nonlinear* functions of $\boldsymbol{u}$ or $\boldsymbol{d}$ will generate the correct moments. Thus, for example, the two-point, second-order spatial correlation tensor can be found from $\hat{\boldsymbol{u}}'$, but the two-point, third-order tensor $\langle u'_i u_j u_k \rangle$ is not in general equal to $\langle \hat{u}'_i u_j u_k \rangle$.

### 3.3. *Linear estimation for homogeneous turbulence*

For the case of homogeneous turbulence the linear estimate is conveniently expressed in terms of $\boldsymbol{x}' = \boldsymbol{x} + \boldsymbol{r}$:

$$\boldsymbol{u}' = \boldsymbol{u}(\boldsymbol{x}+\boldsymbol{r}). \tag{47}$$

Each of the coefficients in (39) is expressed in terms of the two-point spatial correlation tensor

$$R_{li}(\boldsymbol{r}) = \langle u_l(\boldsymbol{x})\, u_i(\boldsymbol{x}+\boldsymbol{r}) \rangle \tag{48}$$

and its derivatives. The necessary relationships are

$$\langle u_l d_{jk} \rangle = \frac{\partial R_{lj}(\mathbf{0})}{\partial r_k}, \tag{49}$$

$$\langle d_{lm} d_{jk} \rangle = -\frac{\partial^2 R_{lj}(\mathbf{0})}{\partial r_k \partial r_m}, \tag{50}$$

$$\langle d_{lm} u_i' \rangle = -\frac{\partial R_{li}(\boldsymbol{r})}{\partial r_m}. \tag{51}$$

Equations (39*a*, *b*) form an $11 \times 11$ system whose coefficient matrix is the same for each component of $u_i'$, $i = 1, 2, 3$. All elements of this matrix involve the two-point spatial correlation and its derivatives evaluated at zero separation. The inverse of the matrix only needs to be evaluated once, independent of $\boldsymbol{r}$ and $i$. Spatial dependencies of the estimation coefficients are determined entirely by the two-point spatial correlations on the right-hand side of (39).

## 4. Homogeneous turbulent shear flow

The linear estimation procedure described in §3 has been used to extract the structure of conditional eddies given local kinematics from a numerical simulation of homogeneous turbulence created by uniform mean shear. Recent work by Rogers & Moin (1987) demonstrates the existence of hairpin structures in homogeneous shear flows in addition to inhomogeneous shear flows. Hairpin eddies have been previously associated with wall-bounded shear flows by numerous authors, beginning with Theodorsen (1952). In numerically simulated channel flow (Kim & Moin 1986) conditional averages based on Willmarth & Lu's (1972) quadrant analysis clearly indicate two types of hairpin structures surrounding burst events: one with its head oriented upwards and downstream of the legs, and the other with its head oriented downwards and upstream of the legs. Similar hairpins have been found in *homogeneous* turbulent shear flow by Rogers & Moin (1987), and from the observations of hairpin eddies with and without walls, they concluded that hairpin structures are a prevalent, if not universal aspect of all turbulent shear flows.

The ubiquitous nature of hairpin vortices in shear flow makes it possible to investigate the relationship between linear estimates of conditional eddies and a reasonably well-defined coherent structure.

### 4.1. *Direct numerical simulation*

The data base used here is the direct numerical simulation of the three-dimensional, time-dependent incompressible Navier–Stokes equation described in Rogers & Moin (1987). The calculations were performed on a grid of $128 \times 64 \times 64$ points using Rogallo's (1981) code and Fourier-spectral methods for representing the velocity field in space. The mean flow was in the $x_1$-direction, and the mean shear was in the $x_2$-direction:

$$U_1 = Sx_2. \tag{52}$$

The computational box, figure 1, was $4\pi \times 2\pi \times 2\pi$ cm in dimension, with $S = 10.0\ \mathrm{s}^{-1}$ and $\nu = 0.045\ \mathrm{cm}^2\ \mathrm{s}^{-1}$, corresponding to the lower Reynolds number reported in Rogers & Moin (1987). The properties of this flow are summarized in table 1. The value of the dimensionless shear $SL_{11,1}/q$ is comparable to that found in the

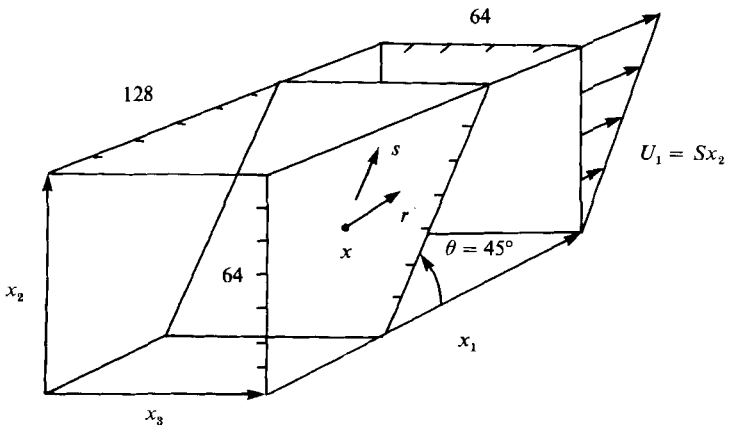


FIGURE 1. Computational domain for homogeneous shear flow.

| | Numerical data $St = 2.0$ | Champagne *et al.* (1970) $St = 3.3$ |
|---|---|---|
| $q\lambda_{11,1}/\nu$ | 14.2 | 250 |
| $qL_{11,1}/\nu$ | 22.2 | 1100 |
| $SL_{11,1}/q$ | 2.66 | 2.0 |
| $Sq^2/\epsilon$ | 3.14 | 5.8 |
| $\langle u_i^2\rangle/q^2$ | (0.43, 0.26, 0.31) | (0.47, 0.25, 0.28) |
| $\langle u_1 u_2\rangle/[\langle u_1^2\rangle \langle u_2^2\rangle]^{\frac{1}{2}}$ | −0.55 | −0.50 |
| $\langle \omega_i^2\rangle^{\frac{1}{2}}/S$ | (0.97, 1.02, 0.82) | — |
| $L_{11,1}/\Delta x$ | 5.23 | — |
| $\lambda_{11,1}/\Delta x$ | 3.35 | — |
| $(\nu/S)^{\frac{1}{2}}/\Delta x$ | 0.68 | — |

TABLE 1. Parameters of the numerical simulation (Rogers & Moin 1987)

experiment of Champagne, Harris & Corrsin (1970), and all computed second-order statistics compare favourably with the experimental data, despite the relatively small Reynolds number of the simulation. ($L_{11,1}$ and $\lambda_{11,1}$ are the longitudinal integral scale and the Taylor microscale respectively, $\Delta x$ is the computational grid, and $q^2$ is twice the turbulent kinetic energy.)

### 4.2. *Estimated CELK eddies*

The linear estimation procedure in (35) and (39) has been used to calculate conditional eddies given the local kinematics from the two-point spatial correlation tensor of the velocity field. Derivatives of $R_{ij}$ in (49), (50) and (51) have been calculated by pseudospectral methods, and the estimation coefficients $A_{ij}(\boldsymbol{r})$ and $B_{ijk}(\boldsymbol{r})$ have been evaluated by solving (39) for each $\boldsymbol{r}$-value on the grid.

#### 4.2.1. *Relationship to coherent structures*

Figure 2 shows the total (mean plus fluctuating) vorticity vector field of a flow realization projected on to an $(x_3, s)$-plane inclined at $\theta = 45°$ to the mean flow direction. Viewing the vorticity vectors in this plane enables one to see a large number of hairpin eddies because the probability distribution of the angle of inclination of the vorticity peaks at $\theta \approx 45°$ and $\theta \approx -135°$ (Rogers & Moin 1987).

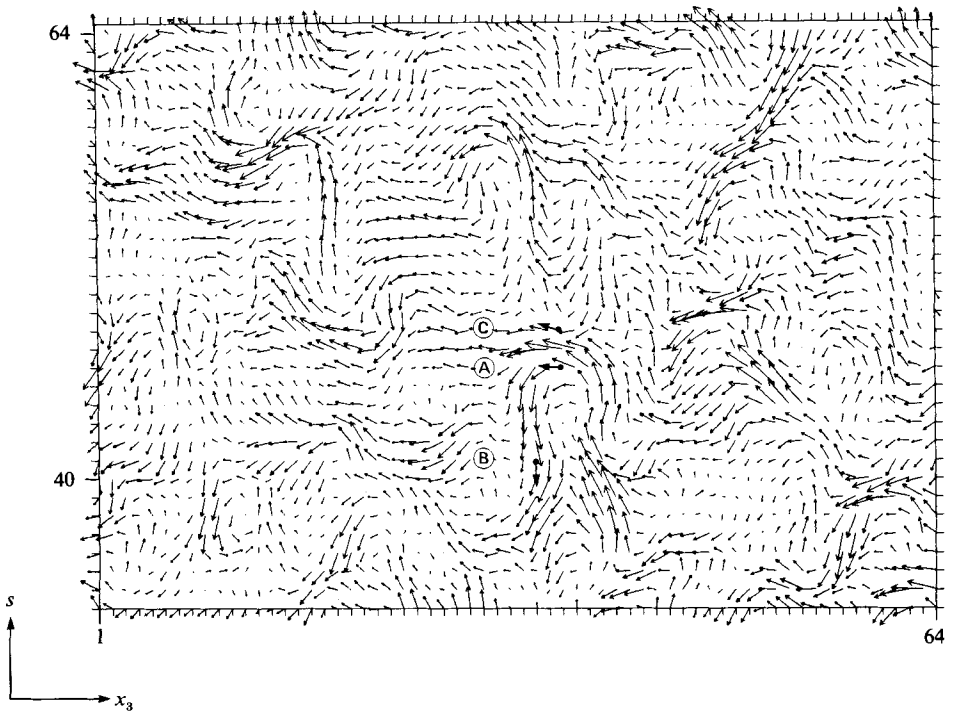


FIGURE 2. Vorticity vector field of homogeneous shear flow projected onto a plane inclined at $\theta = 45°$ (see figure 1) and passing through $x_1 = 0$. The conditional event $\boldsymbol{E}_{u,d}$ is evaluated at points A, B and C. The numbers on the axes indicate grid points (see table 1). Note that the spacing of the tic marks on the vertical axis is equal to $\sqrt{2}\Delta x$.

Several hairpins are contained in figure 2. In this and all subsequent vector plots the numbers on the coordinate axes indicate the grid points (see table 1).

To study the relationship between instantaneous coherent structures and linearly estimated CELK eddies, a hairpin was selected from figure 2, and the flow conditions $\{\boldsymbol{u}, \boldsymbol{d}\}$ at points labelled A, B and C were used to calculate the conditional eddy. Point A is near the centre of the vortex tube at the head of the hairpin, and its fluctuating vorticity is $\boldsymbol{\omega}(\boldsymbol{x}) = (-1.22, 1.94, -15.45)\ \mathrm{s}^{-1}$. The mean vorticity is $\boldsymbol{\Omega} = (0, 0, -10)\ \mathrm{s}^{-1}$. The total vorticity is dominated by a strongly negative $\omega_3$-component, corresponding to the nearly horizontal total vorticity vector at the top of the hairpin at Point A. The velocity $\boldsymbol{u}(\boldsymbol{x}) = (-4.50, 2.29, -0.65)\ \mathrm{cm\ s}^{-1}$ lies in the second quadrant of the $(u_1, u_2)$-plane, and the largest and smallest elements in the fluctuating deformation tensor at point A are $d_{12} = 13.2\ \mathrm{s}^{-1}$ and $d_{23} = 0.4\ \mathrm{s}^{-1}$, respectively.

Figure 3 shows the vorticity field of the linear estimate given the conditions at point A

$$\hat{\boldsymbol{\omega}}' = \boldsymbol{\nabla}' \times \hat{\boldsymbol{u}}'. \tag{53}$$

plus the mean vorticity $\boldsymbol{\Omega}$. Projection into a 45° plane reveals a characteristic hairpin pattern very similar to the realization in figure 2.

Vortex lines computed from

$$\frac{\mathrm{d}\boldsymbol{r}}{\mathrm{d}l} = \frac{(\hat{\boldsymbol{\omega}}' + \boldsymbol{\Omega})}{|\hat{\boldsymbol{\omega}}' + \boldsymbol{\Omega}|} \tag{54}$$

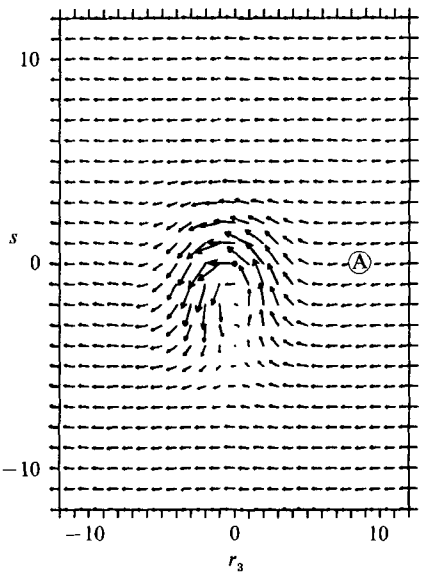


FIGURE 3. Linearly estimated total vorticity field of a CELK eddy evaluated for the conditions at Point A in figure 2. The vorticity vector is projected onto a plane inclined at $\theta = 45°$ (see figure 2) and passing through point A. The tic marks on the axes represent grid points (see table 1).

are shown in figure 4. In this depiction the total vorticity field gives the impression of a vortex sheet that has been perturbed upwards. For comparison, figure 5 shows the vortex lines computed by Kim & Moin (1986) by conditionally sampling the velocity in numerically simulated channel flow. They used a second-quadrant detector ('QD-2') at $y^+ = 100$, wherein the instantaneous Reynolds stress exceeded ten times the mean. The similarity between the vorticity of the linearly estimated field in figure 4(*a*) and conditionally sampled field is striking. It was also shown in Kim & Moin (1986) that other detector events such as the variable-interval space-averaging (VISA) event yielded related structures, although the VISA event appeared to occur in a region between an upwards and a downwards depression of the vortex sheet. This and our recent application of linear estimation in channel flow leads us to conclude that the linearly estimated CELK eddy is close in form to the conditional averages that have been most commonly observed in the past.

### 4.2.2. *Effect of the conditions*

The kinematic conditions at Point B in figure 2 correspond to the left leg of the upwards hairpin. The fluctuating vorticity is large and negative in the $x_1$- and $x_2$-directions, and it nearly cancels the mean vorticity in the $x_3$-direction: $\boldsymbol{\omega}(\boldsymbol{x}) = (-7.76, -26.58, 10.2)\ \mathrm{s}^{-1}$. The velocity vector $\boldsymbol{u}(\boldsymbol{x}) = (-0.94, -0.53, -0.52)\ \mathrm{cm\ s}^{-1}$ has $u_1$- and $u_2$-components that are weak relative to those at Point A.

The conditions at Point B produce a linearly estimated CELK eddy that emphasizes the left leg of the hairpin, figure 6. The point $\boldsymbol{r} = 0$ now appears to be centred on the left leg at about the same point as the location of Point B relative to the instantaneous realization of the hairpin in figure 2. The left leg in figure 6(*a*) is slightly more pronounced than in figure 3 because specifying data corresponding to the left leg yields a better stochastic estimate of the flow in this region (i.e. smaller mean-square error). However, the right leg is significantly less pronounced than in

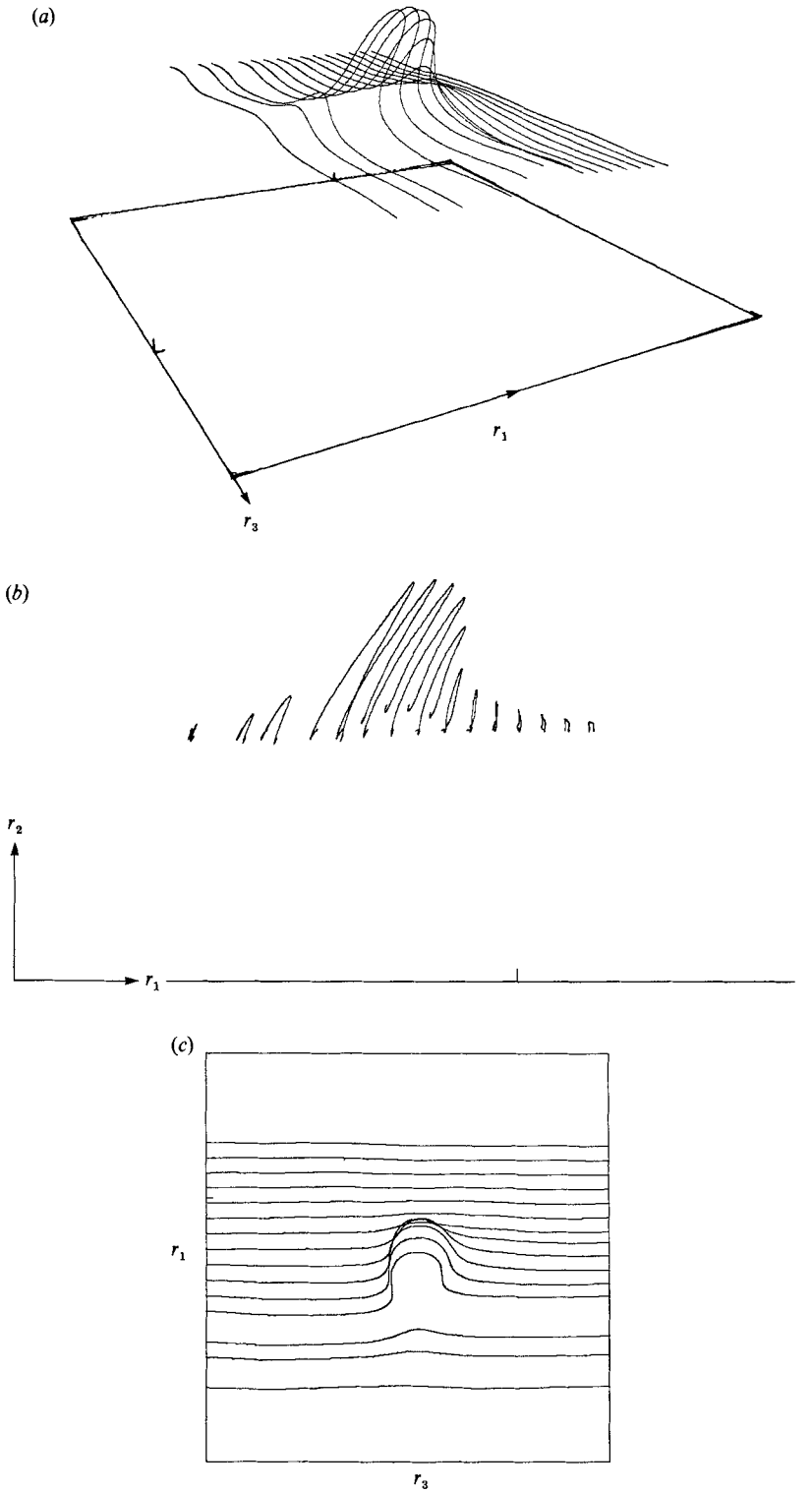


FIGURE 4. Vortex lines of the CELK eddy for the conditions at Point A in the homogeneous shear flow. (*a*) Oblique view; (*b*) side view; (c) top view.

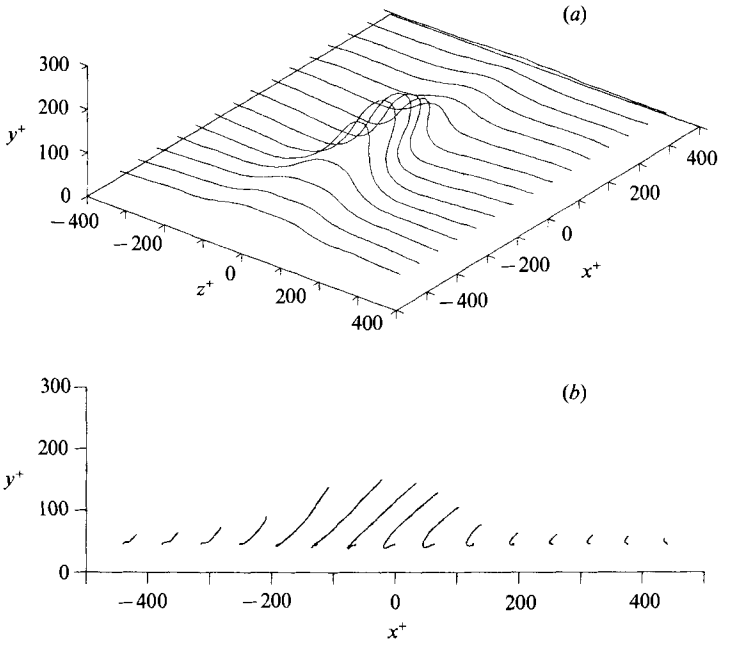


FIGURE 5. Vortex lines of a conditional ensemble average based on a quadrant-2 conditional event in turbulent channel flow. (*a*) Oblique view; (*b*) side view (Kim & Moin 1986).

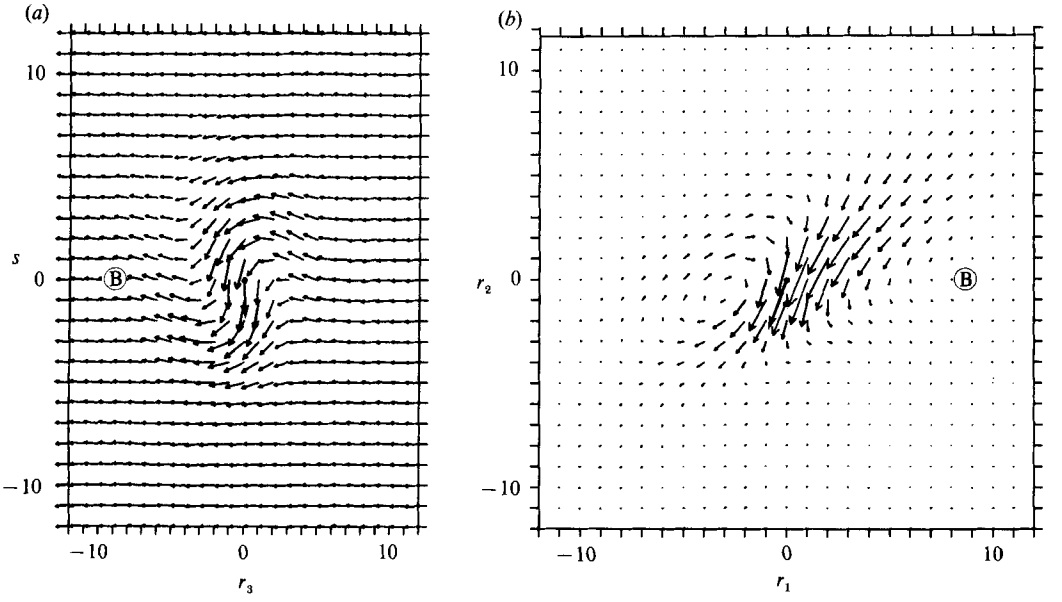


FIGURE 6. Linearly estimated total vorticity field of a CELK eddy evaluated for the conditions at Point B in figure 2. (*a*) Vorticity projected onto the plane inclined at $\theta = 45°$ (see figure 1) and passing through point B; (*b*) vorticity projected onto the $(r_1, r_2)$-plane passing through Point B.

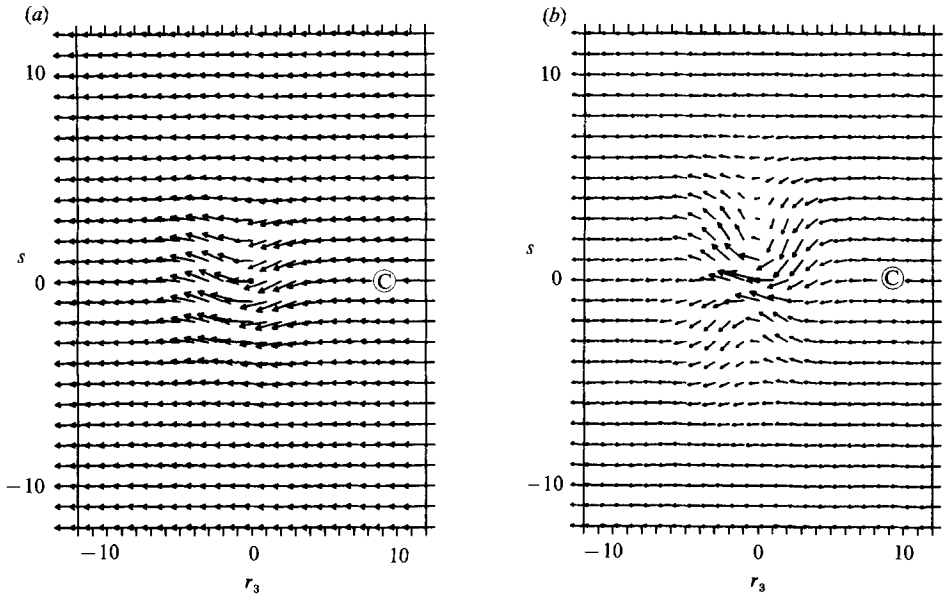


FIGURE 7. Linearly estimated total vorticity field of a CELK eddy evaluated for the conditions at Point C in figure 2. Vorticity errors on a $\theta = 45°$ plane. (*a*) Estimation given $\boldsymbol{u}(\boldsymbol{x})$; (*b*) estimation given $\boldsymbol{u}(\boldsymbol{x})$ and $\boldsymbol{d}(\boldsymbol{x})$.

figure 3. This loss of structure is the consequence of reduced correlation between the flow in the region of the right leg and the data at $\boldsymbol{r} = 0$. In general, as $|\boldsymbol{r}|$ increases the flows predicted by the linear estimates must attenuate if the two-point spatial correlation functions decay. A similar effect is also observed for the conditional average, and it is merely a consequence of loss of correlation. It should be noted that the pattern in figure 6(*a*) could also represent the right leg of a downwards-oriented hairpin which would also possess vorticity with the same direction as the left leg of an upwards hairpin.

In figure 6(*b*) a side view of the linear estimate around Point B shows that the pattern corresponds to a bundle of vortex lines oriented at approximately $-135°$ to the flow. It is noteworthy that while the vorticity vector at $\boldsymbol{x}$ is inclined at $-106°$, the main structure of the vortex bundle is inclined at about $-135°$, the angle of maximum probability found by Rogers & Moin (1987).

At Point C the velocity is relatively small, $\boldsymbol{u}(\boldsymbol{x}) = (0.96, -0.38, 0.23)$ cm s$^{-1}$ and the fluctuating vorticity is a combination of a moderate total $\omega_3$-component coupled with a strong fluctuation in the streamwise direction: $\boldsymbol{\omega}(\boldsymbol{x}) = (6.40, 2.19, -12.84)$ s$^{-1}$. The complete deformation tensor of the fluctuating field is

$$d_{ij}(\boldsymbol{x}) = \begin{pmatrix} 4.53 & 10.33 & 4.02 \\ -2.51 & -9.51 & -3.56 \\ 1.83 & 2.84 & 4.98 \end{pmatrix}. \tag{55}$$

From figure 2, Point C appears to be midway between the head of an upward hairpin and the head of a downward hairpin.

To assess the extent to which specification of the full kinematic state $\boldsymbol{E}_{\boldsymbol{u},\boldsymbol{d}}$ improves estimation of the local structure, the flow around Point C has been linearly estimated given $\boldsymbol{u}$ in figure 7(*a*) and given $\{\boldsymbol{u}, \boldsymbol{d}\}$ in figure 7(*b*). The vorticity vectors in figure

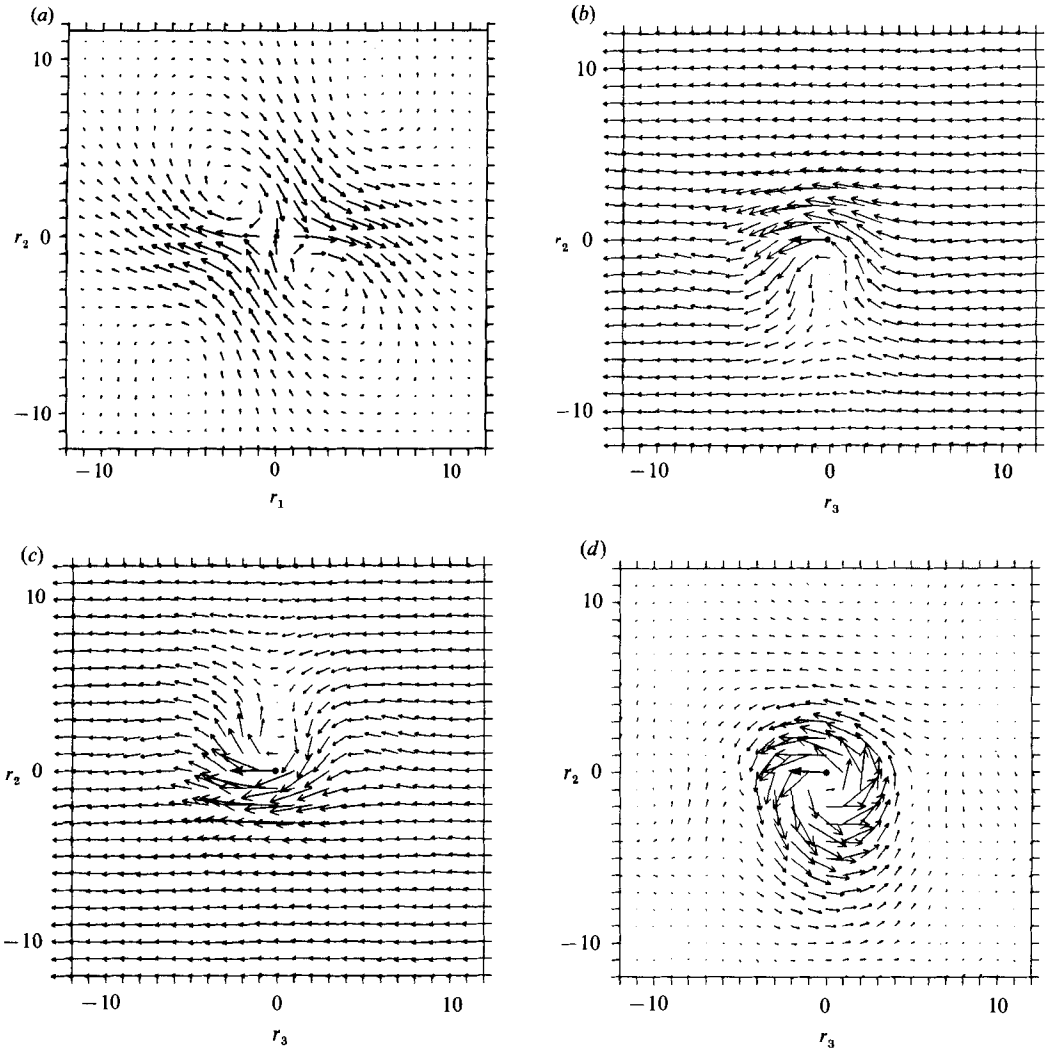


FIGURE 8. Linearly estimated CELD velocity field. $\boldsymbol{u}(\boldsymbol{x}) = 0, d_{11}(\boldsymbol{x}) = 20, d_{22}(\boldsymbol{x}) = -20$. (*a*) Velocity vectors in the $r_3 = 0$ plane; (*b*) total-vorticity vectors in the $r_1 = -3\Delta x$ plane; (*c*) total-vorticity vectors in the $r_1 = 3\Delta x$ plane; (*d*) fluctuating vorticity in the $r_1 = -3\Delta x$ plane.

7(*a*) are computed from a $3 \times 3$ system of equations for the linear estimation coefficients, and they show relatively little structure. In contrast, the linear estimate in figure 7(*b*), computed from the full $11 \times 11$ system, indicates the presence of two hairpins configured head-to-head. The point $\boldsymbol{r} = 0$ is located midway between them, as expected from figure 2. We conclude that under certain conditions the information contained in $\boldsymbol{d}(\boldsymbol{x})$ is necessary to produce a clear, representative pattern for the local field, in agreement with the observation of Ditter (1987).

An extreme situation in which the deformation tensor provides essential information occurs when the velocity vanishes at $\boldsymbol{x}$. Then, $\boldsymbol{x}$ is a critical point of the vector field. The linearly estimated field of the CELT eddy vanishes identically, and the field of the CELK eddy reduces to that of a CELD eddy. The CELD flow pattern corresponding to an arbitrarily chosen pure two-dimensional strain, $\boldsymbol{u}(\boldsymbol{x}) = \boldsymbol{0}$,

$d_{11}(\boldsymbol{x}) = 20$, $d_{22}(\boldsymbol{x}) = -20$, is shown in figure 8(*a*). In the immediate vicinity of $\boldsymbol{x}$ the flow is a plane stagnation-point flow. Farther from $\boldsymbol{x}$ the pattern is that of the heads of two hairpin vortices located on either side of $\boldsymbol{x}$ (figure 8*b*, *c*). The stagnation point occurs where the induced motions of the vortices cancel. Such points presumably have high positive pressure fluctuations associated with them. They illustrate the 'splat' mechanism for generating pressure fluctuations discussed by Bradshaw & Koh (1981), and they are potential sites for the creation of acoustic emission.

It is noteworthy that vorticity-fluctuation vectors depict ring vortices rather than hairpins (figure 8*d*) (see Falco 1977, and Moin, Leonard & Kim 1986). In this regard, Ditter (1987) has found that the addition of a mean shear flow to the vortex ring found by linear estimation of isotropic turbulence yields a hairpin vortex. The mean vorticity adds to the vorticity of one side of the ring vortex and cancels the vorticity on the other side. Thus, the relative strengths of the fluctuating vorticity and mean shear (and the frame of reference) are important parameters that affect the appearance of organized structures in this flow.

Comparing figures 3, 4, 6, 7 and 8, we see that the effects of selecting a specific event are two-fold. First, if two conditional events each occur within the same structure, then the effect of the event is to 'focus' the linear estimate on a region centred upon the point at which the event occurs, on average. The difference between Points A and B in figures 3 and 6 illustrates this behaviour. Secondly, if any two conditional events are not part of the *same* structure, then a new structure can be revealed. The stagnation-point flow in figure 8 illustrates a new mechanism that is not clearly evident in the individual hairpins. Physically, if a flow is dominated by a single characteristic structure, then one expects to see only one conditional structure, or perhaps interactions between the structures. It should be emphasized that without additional evidence (which would depend upon the specific flow) the estimated eddies must always be interpreted as averages that may not coincide too closely to any single realization, especially when the flow at $\boldsymbol{x}'$ is not highly correlated with the flow at $\boldsymbol{x}$.

It should also be noted that different events may be associated with different *phases* of a particular interaction, so that it is possible to obtain an evolving picture of the flow around the point $\boldsymbol{x}$ by using a proper sequence of values for $\boldsymbol{u}(\boldsymbol{x})$. (The movie by Adrian, Jones & Hassan (1979) used time-series measurements of $u_1(\boldsymbol{x}, t)$ and $u_2(\boldsymbol{x}, t)$ to produce a series of linearly estimated flow fields as a function of time in turbulent pipe flow.)

### 4.3. *Reynolds-shear-stress events*

The conditional eddy together with the probability density function of the conditional event are both necessary to describe coherent structures, because the former describes the flow geometry and kinematics associated with an event, while the latter describes the relative frequency of that event. Without an *a priori* criterion for selecting a particular event one should, strictly, examine all possible events. Practically, it is necessary to devise a procedure that limits the number of interesting events to a feasibly small set. A natural approach to this problem is to select events on the basis of the amount that they contribute to quantities of particular physical interest such as kinetic energy, Reynolds shear stresses, or dissipation. The method is based on the equation for the unconditional mean value

$$\langle \boldsymbol{Q}(\boldsymbol{u}, \boldsymbol{d}) \rangle = \int \boldsymbol{Q}(\boldsymbol{v}, \boldsymbol{A}) f_{\boldsymbol{ud}}(\boldsymbol{v}, \boldsymbol{A}; \boldsymbol{x}, t)\, \mathrm{d}\boldsymbol{v}\, \mathrm{d}\boldsymbol{A}, \tag{56}$$

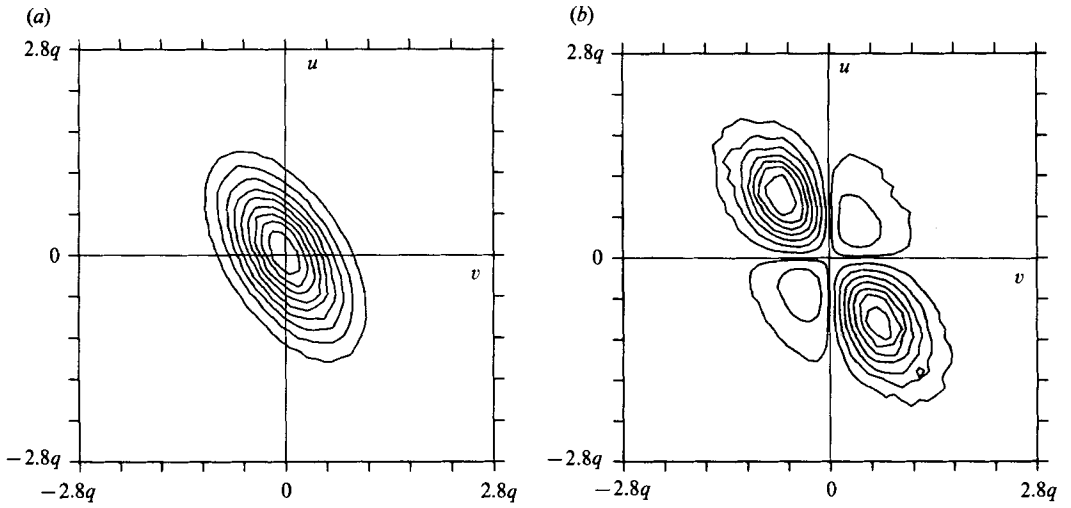


FIGURE 9. Events making the greatest contribution to $\langle \boldsymbol{u}_1 \boldsymbol{u}_2 \rangle$. (*a*) Contours of $f_{u_1 u_2}(v_1, v_2)$; (*b*) contours of $v_1 v_2 f_{u_1 u_2}(v_1, v_2)$: $q = 1.94$ cm s$^{-1}$.

which indicates that the maximum contribution to $\langle \boldsymbol{Q} \rangle$ is derived from those $\{\boldsymbol{u}, \boldsymbol{d}\}$ events for which the integrand $\boldsymbol{Q} f_{\boldsymbol{ud}}$ is a maximum. Relative maxima may occur at several points in $(\boldsymbol{v}, \boldsymbol{\Delta})$-space. We shall refer to the events corresponding to these points as maximum contributors.

In this section the flow structures associated with a maximum contributor to the Reynolds shear stress, given by

$$\langle u_1 u_2 \rangle = \int v_1 v_2 f_{\boldsymbol{ud}}(\boldsymbol{v}, \boldsymbol{\Delta}; \boldsymbol{x}, t)\, \mathrm{d}\boldsymbol{v}\, \mathrm{d}\boldsymbol{\Delta} \tag{57a}$$

$$= \int v_2 v_2 f_{\boldsymbol{u}}(\boldsymbol{v}; \boldsymbol{x}, t)\, \mathrm{d}\boldsymbol{v}, \tag{57b}$$

will be investigated. The variables $\boldsymbol{u}$, $\boldsymbol{d}$ and the associated dummy variables $\boldsymbol{v}$, $\boldsymbol{\Delta}$ will continue to represent fluctuations about the mean. In principle, the points in $(\boldsymbol{v}, \boldsymbol{\Delta})$-space at which $v_1 v_2 f_{\boldsymbol{ud}}$ is a maximum can be determined by straightforward search of the numerical solution, provided that the data base is large enough to yield a statistically significant population in the pertinent phase-space cells. For the present calculation it was desirable to reduce the dimension of $(\boldsymbol{v}, \boldsymbol{\Delta})$-space to improve the statistical stability of the samples. Reduction was accomplished by observing that by virtue of homogeneity in the $(x_1, x_2)$-plane, the following moments vanish identically: $\langle u_1 u_3 \rangle$, $\langle u_2 u_3 \rangle$, $\langle u_1 d_{13} \rangle$, $\langle u_2 d_{13} \rangle$, $\langle u_1 d_{31} \rangle$, $\langle u_2 d_{31} \rangle$, $\langle u_1 d_{23} \rangle$, $\langle u_2 d_{23} \rangle$, $\langle u_1 d_{32} \rangle$ and $\langle u_2 d_{32} \rangle$. Hence, $u_3$, $d_{13}$, $d_{31}$, $d_{23}$ and $d_{32}$ are each uncorrelated with the variables $u_1$ and $u_2$. While lack of correlation does not guarantee statistical independence, it does suggest that $u_3$, $d_{13}$, $d_{31}$, $d_{23}$ and $d_{32}$ are not strongly coupled to the events contributing most to $\langle u_1 u_2 \rangle$. They were therefore ignored, leaving the variables $u_1$, $u_2$, $d_{11}$, $d_{12}$, $d_{21}$ and $d_{22}$ to be considered.

The two-dimensional probability density of velocity for the homogeneous shear flow is plotted in figure 9(*a*), and contours of $v_1 v_2 f_{\boldsymbol{u}}(v_1, v_2)$ are shown in figure 9(*b*). It is seen that maxima occur in the bins centred at $(v_{m1}, v_{m2}) = (-1.65, 1.21)$ cm s$^{-1}$ and $(1.65, -1.21)$ cm s$^{-1}$. (Note that for a large statistical sample the entire probability distribution should be symmetric with respect to reflections in

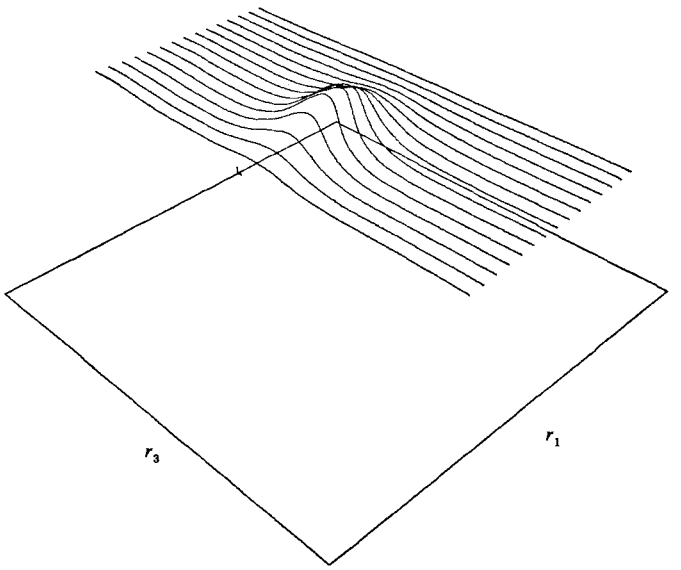


FIGURE 10. Vortex lines of the CELK eddy making the peak second-quadrant contribution to $\langle u_1 u_2 \rangle$. Linear estimate using $\boldsymbol{u} = (-1.61, 1.21, 0)$ cm s$^{-1}$, and $\boldsymbol{d} = 0$.

homogeneous shear flow.) The maxima are located in the second and fourth quadrants, and they correspond, *in this sense*, to the sweep and ejection events of wall-bounded turbulent shear flow.

The four-dimensional conditional probability density of deformation $f_{\boldsymbol{d}}(d_{11}, d_{12}, d_{21}, d_{22} | v_{m1}, v_{m2})$ has also been computed. Its maximum was found at zero deformation, indicating that the most probable state of the maximum Reynolds-stress contributor is $(v_1, v_2, d_{11}, d_{12}, d_{21}, d_{22}) = (v_{m1}, v_{m2}, 0, 0, 0, 0)$.

The flow field of the second-quadrant Reynolds-shear-stress event has been linearly estimated using $\boldsymbol{u}' = \boldsymbol{A}\boldsymbol{u} + \boldsymbol{B}\boldsymbol{d}$ and setting $\boldsymbol{u} = (-1.65, 1.21, 0)$, and $\boldsymbol{d} = 0$. The vortex lines in figure 10 reveal a structure very similar to the patterns that were associated with hairpins in figures 4 and 5. Total vorticity vectors projected onto $(r_1, r_2)$-planes are shown in figure 11. In the $r_3 = 0$ plane the projected vorticity is zero at every point, indicating that vorticity is perpendicular to the plane. As $r_3$ is changed, patterns emerge that are clearly identifiable as the legs of a hairpin vortex. The projected vorticity reaches a maximum at $|r_3| = 2\Delta x$ and decreases thereafter. The vorticity pattern is symmetric with respect to the $r_3 = 0$ plane, aside from a change in its sign. The total pattern of vorticity is consistent with an upwards-oriented hairpin vortex inclined at about $\theta = 55°$ to the flow.

The velocity field of the Reynolds-stress eddy is projected onto an $(r_2, r_3)$-plane passing through $\boldsymbol{r} = 0$ in figure 12(*a*). The vortical patterns on either side of $\boldsymbol{r} = 0$ are cuts through the legs of the hairpin. The vorticity is concentrated in the legs, showing that the pattern is more like a vortex tube bent into a hairpin shape than the perturbed-vortex-sheet impression given by figure 12. At $\boldsymbol{r} = 0$ the fluctuating velocity vector is a strong flow inclined at $\theta = 143°$ to the streamwise direction. The local instantaneous Reynolds stress produced at $\boldsymbol{r} = 0$ is $u_1(\boldsymbol{x})\, u_2(\boldsymbol{x}) = -2.0$ cm$^2$ s$^{-2}$, corresponding to approximately 3 $\langle u_1 u_2 \rangle$. The strength of the flow at $\boldsymbol{r} = 0$ is associated with *mutual induction by the vorticity in the head and legs of the hairpin vortex*. The point $\boldsymbol{r} = 0$ is located about the same distance below the head of the

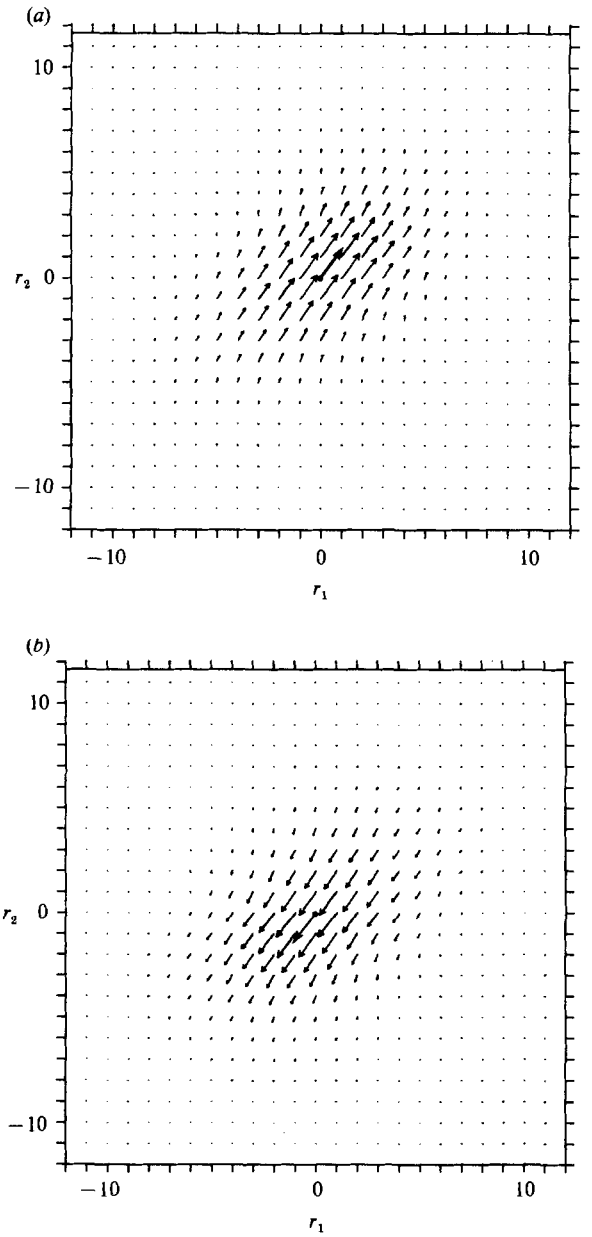


FIGURE 11. Vorticity field of the CELK eddy making the peak second-quadrant contribution to $\langle u_1 u_2 \rangle$. Linear estimate projected onto the $(r_1, r_2)$-plane. (*a*) $r_3 = +2\Delta x$; (*b*) $r_3 = -2\Delta x$.

hairpin as it is from the side legs. Hence, the flow at $\boldsymbol{r} = 0$ benefits about equally from vortex induction by all parts of the surrounding vortex tube. The consequence of this cooperative induction is a negative $u_1 u_2$-event that is much stronger than the positive $u_1 u_2$ events associated with the weaker return flows on the outside of the hairpin. In this way, a net negative value of $\langle u_1 u_2 \rangle$ is produced.

The velocity-fluctuation field under the head of the conditional hairpin is shown projected onto the $(r_1, r_2)$-plane passing through $\boldsymbol{r} = 0$ in figure 12(*b*). The head of the hairpin is located at about $r_1 = 5\Delta x$, $r_2 = 5\Delta x$. Fluid is drawn into the hairpin for a

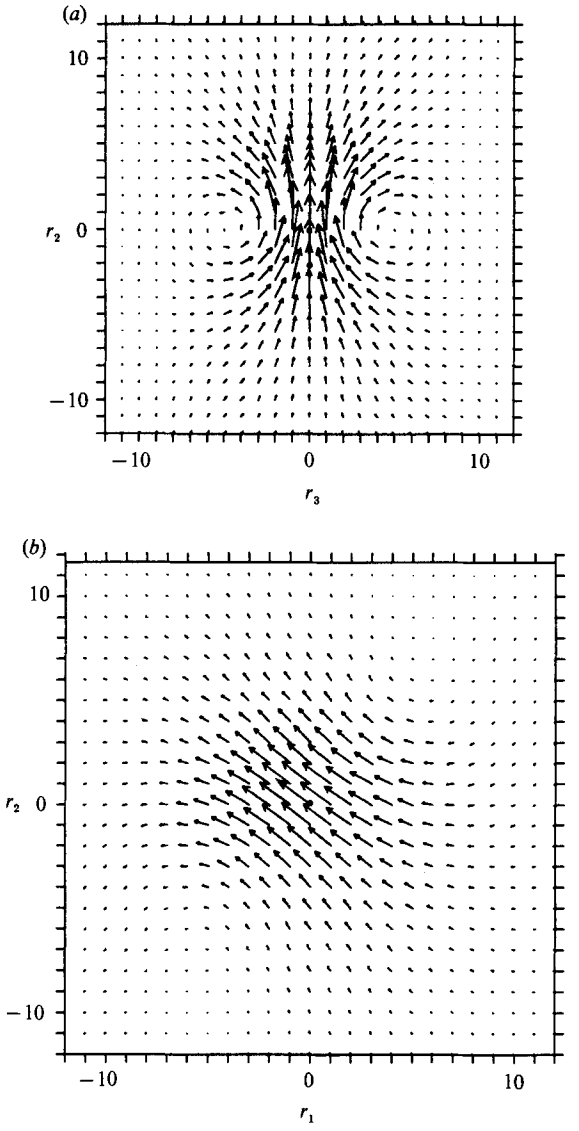


FIGURE 12. Velocity field of the peak second-quadrant Reynolds-stress event. (*a*) projected onto the $(r_2, r_3)$-plane, $r_1 = 0$; (*b*) projected onto the $(r_1, r_2)$-plane, $r_3 = 0$.

significant distance ahead of it. Patterns in the vector field far away from $\boldsymbol{r} = 0$ are subject to sampling-error noise in the two-point spatial correlations, and they may not be reliable.

The fourth-quadrant peak contribution to $\langle u_1 u_2 \rangle$ occurs at values of $u_1$ and $u_2$ that are opposite to those of the second-quadrant event, figure 9(*b*). From the form of the linear estimate with $\boldsymbol{d} = 0$ it is clear that inverting the given velocity vector simply inverts all of the vectors in the estimated field. Thus, the conditional eddy associated with the fourth-quadrant event is a downwards-oriented hairpin. More generally, the patterns associated with other $\boldsymbol{v}_1 - \boldsymbol{v}_2$ values not too far from the locations of the maximum contributions are expected to correspond to hairpins whose legs are approximately perpendicular to the given velocity (J. L. Ditter &

R. J. Adrian 1988, paper in preparation). A picture emerges in which second- and fourth-quadrant Reynolds stresses are generated primarily by groups of upward and downward hairpins inclined at a range of angles about mean values of approximately 45° and −135° to the flow. The angular distribution of vorticity in $(x_1, x_2)$-planes found by Rogers & Moin (1987) indicates how this distribution may occur.

## 5. Summary and conclusions

A new type of conditional eddy has been defined by the conditional average $\langle \boldsymbol{u}(\boldsymbol{x}', t) \,|\, \boldsymbol{u}(\boldsymbol{x}, t), \boldsymbol{d}(\boldsymbol{x}, t) \rangle$ in which the conditional event specifies the local kinematic state at $\boldsymbol{x}$ in terms of the velocity and the deformation. The additional specification of the local deformation permits a more precise determination of the fluid motion.

The equation governing the probability density function of the kinematic state $f_{\boldsymbol{u},\boldsymbol{d}}$ has been derived for constant-property, incompressible flow. All evolution equations governing moments defined by $\boldsymbol{u}(\boldsymbol{x}, t)$ and $\boldsymbol{d}(\boldsymbol{x}, t)$ are contained within this equation and, in particular, the equations used in turbulence modelling such as those governing the Reynolds stresses, mean-square vorticity and dissipation can be derived from it. Closure of the equation for $f_{\boldsymbol{u},\boldsymbol{d}}$ requires approximation of the conditional velocity $\langle \boldsymbol{u}' \,|\, \boldsymbol{u}, \boldsymbol{d} \rangle$. In this way the probability-density-function equation provides a link between coherent flow structures corresponding to the conditional eddies and the modelling of turbulent transport.

Approximation of the conditional eddies given the local kinematics has been accomplished by mean-square stochastic estimation in terms of data linear in $\boldsymbol{u}(\boldsymbol{x}, t)$ and $\boldsymbol{d}(\boldsymbol{x}, t)$. The linear-estimation coefficients are calculated from a simple system of linear algebraic equations involving only the two-point spatial correlation functions of the velocity. The estimation procedure is an effective method of using spatial correlation information to obtain readily interpretable velocity fields corresponding to large-scale structures. It avoids time-consuming conditional-sampling procedures.

In the immediate vicinity of $\boldsymbol{x}$ the conditional events $\boldsymbol{u}(\boldsymbol{x}, t)$ and $\boldsymbol{d}(\boldsymbol{x}, t)$ provide information sufficient to estimate the local velocity field by a Taylor-series expansion to first order:

$$u_i(\boldsymbol{x}', t) = u_i(\boldsymbol{x}, t) + d_{ij}(\boldsymbol{x}, t)\,(x_j' - x_j). \tag{58}$$

If $\boldsymbol{u}(\boldsymbol{x}, t) = 0$, $\boldsymbol{x}$ is a critical point, and critical-point analysis provides further information about the local topology of the vector field. The linear stochastic estimate (and the conditional average $\langle \boldsymbol{u}' \,|\, \boldsymbol{u}, \boldsymbol{d} \rangle$) is also a local approximation, but it clearly contains more structural information than either of the foregoing analyses. In particular, the stochastic estimate contains information about the size, shape, and orientation of the local eddies that cannot be inferred from critical-point analysis based on a single critical point at $\boldsymbol{x}$. Critical-point analysis does not distinguish between topologically equivalent vector fields, whereas the shape information contained in the spatial correlation tensor is capable of defining many differently shaped, but topologically equivalent, structures. Conversely, two different spatial correlation functions can produce topologically different fields given the same critical point. While these considerations are an attempt to delineate the differences between critical-point analysis and stochastic estimation, they also suggest that it may be useful to specify conditional events at the critical points. However, it should be noted that the hairpin structure associated with the maximum Reynolds-stress contribution arose from a velocity condition at a point where $\boldsymbol{d}$ vanished. It should

finally be noted that the mean-square error of (54) grows without bound as $|\boldsymbol{x}'-\boldsymbol{x}| \to \infty$, but the mean-square error of a stochastic estimate is bounded by the mean square of the velocity fluctuation.

Using correlations computed from a direct numerical simulation of homogeneous turbulent shear flow, it is found that one conditional-eddy structure characteristic of this type of flow is a hairpin vortex. The linearly estimated conditional eddy corresponds closely in shape to instantaneous hairpins found in the numerical simulation and to hairpins inferred from conditional averages. The linear estimate is, therefore, a good approximation of the conditional average on large scales. The large-scale structure inferred from the linear estimate is not necessarily sensitive to the choice of conditional events. If two different events each occur within the same coherent eddy structure, the linearly estimated patterns are merely shifted so as to be centred on the points at which the events occur, on average. In some cases, events may define a new structure, different from the primary (i.e. most common) structure.

A rational method of selecting events is proposed based on determining the values of $\boldsymbol{u}, \boldsymbol{d}$ at which the greatest contribution to some mean quantity occurs. Using the mean Reynolds shear stress as a criterion, it is found that two events exhibit maxima in their contributions: a second-quadrant event and a fourth-quadrant event. The linearly estimated conditional eddy associated with the second-quadrant event is a hairpin vortex inclined upwards and in the streamwise direction at about 45° to the mean flow, and that for the fourth-quadrant event is a similar eddy inclined downwards at $-135°$ with respect to the positive flow direction. The patterns inferred from the linear estimates indicate that the peak contribution to Reynolds stresses in homogeneous turbulent shear flow comes from fluid jetting through the region below the head of the vortex in a direction almost perpendicular to the plane of the hairpin. This strong jet is a consequence of vortex induction by the opposing legs of the hairpin reinforced by induction from vorticity in the head of the hairpin. Since hairpins are observed in wall-bounded inhomogeneous flows as well as homogeneous shear flow, it is not unlikely that this mechanism for creating Reynolds stresses is a common feature of all shear flows.

This research was supported by NASA-Ames Joint Research Interchange NCA2-1R330-401 and NCA2-131. We thank Dr Michael Rogers for helpful discussions.

## REFERENCES

ADRIAN, R. J. 1975 On the role of conditional averages in turbulence theory. In *Proc. Fourth Biennial Symp. on Turbulence in Liquids, Sept. 1975*. University of Missouri-Rolla. Also in *Turbulence in Liquids* (1977), p. 323. Science.

ADRIAN, R. J. 1978 Structural information obtained from analysis using conditional vector events: A potential tool for the study of coherent structures. In *Coherent Structure of Turbulent Boundary Layers* (ed. C. R. Smith & D. E. Abbott), pp. 416–421. Lehigh Univ., Bethlehem, PA.

ADRIAN, R. J. 1979 Conditional eddies in isotropic turbulence. *Phys. Fluids* **22**, 2065.

ADRIAN, R. J., JONES, B. G. & HASSAN, Y. A. R. 1979 *Conditional Eddies in Turbulent Pipe Flow*. 8 mm film. University of Illinois, Urbana.

ANTONIA, R. A. 1981 Conditional sampling in turbulence measurement. *Ann. Rev. Fluid Mech.* **13**, 131.

BAKEWELL, H. P. & LUMLEY, J. L. 1967 Viscous sublayer and adjacent wall region in turbulent pipe flow. *Phys. Fluids* **10**, 1880.

BLACKWELDER, R. F. & KAPLAN, R. E. 1976 On the wall structure of the turbulent boundary layer. *J. Fluid Mech.* **76**, 89.

BRADSHAW, P. & KOH, Y. M. 1981 A note on Poisson's equation for pressure in a turbulent flow. *Phys. Fluids* **24**, 777.

CANTWELL, B. 1981 Organized motion in turbulent flow, *Ann. Rev. Fluid Mech.* **13**, 457.

CHAMPAGNE, F. H., HARRIS, V. G. & CORRSIN, S. 1970 Experiments on nearly homogeneous shear flow. *J. Fluid Mech.* **41**, 81.

CHANG, P., ADRIAN, R. J. & JONES, B. G. 1985 Fluctuating pressure and velocity fields in the near field of a round jet. *Theor. and Appl. Mech. Dept, University of Illinois, Rep.* 475. UILU-ENG 85-6006.

DITTER, J. L. 1987 Stochastic estimation of eddies conditioned on local kinematics: isotropic turbulence. M.S. thesis, Dept of Theor. and Appl. Mech., University of Illinois, Urbana, Illinois.

FALCO, R. E. 1977 Coherent motions in the outer region of turbulent boundary layers. *Phys. Fluids* **20**, S124.

HASSAN, Y. A. R. 1980 Experimental and modeling studies of two-point stochastic structure in turbulent pipe flow. Ph.D. thesis, Nuclear Engr. Prog., University of Illinois, Urbana.

HASSAN, Y. A. R., JONES, B. G. & ADRIAN, R. J. 1987 Two-point stochastic structure in turbulent pipe flow. *Nuclear Thermal-Hydraulics Rep.* 2. UILU-ENG, 87-5302, University of Illinois, Urbana, IL.

HUSSAIN, A. K. M. F. 1983 Coherent structures – reality and myth. *Phys. Fluids* **26**, 2816.

KIM, J. & MOIN, P. 1986 The structure of the vorticity field in turbulent channel flow. Part 2. Study of ensemble-averaged fields. *J. Fluid Mech.* **162**, 339.

LUMLEY, J. L. 1970 *Stochastic Tools in Turbulence.* Academic.

LUMLEY, J. L. 1981 Coherent structures in turbulence. In *Transition and Turbulence* (ed. R. E. Meyer), pp. 215–241. Academic.

LUNDGREN, T. S. 1967 Distribution functions in the statistical theory of turbulence. *Phys. Fluids* **10**, 969.

MOIN, P. 1984 Probing turbulence via large eddy simulation. *AIAA Paper* 84-0174.

MOIN, P. & KIM, J. 1985 The structure of the vorticity field in turbulent channel flow. Part 1. Analysis of instantaneous fields and statistical correlations. *J. Fluid Mech.* **155**, 441.

MOIN, P., LEONARD, A. & KIM, J. 1986 Evolution of a curved vortex filament into a vortex ring. *Phys. Fluids* **29**, 955.

NITHIANANDAN, C. K. 1980 Fluctuating velocity pressure field structure in a round jet turbulent mixing region. Ph.D. thesis, Nuclear Engr. Prog., University of Illinois, Urbana, IL.

NITHIANANDAN, C. K., JONES, B. G. & ADRIAN, R. J. 1987 Turbulent velocity pressure field structures in an axisymmetric mixing layer. *Nuclear Thermal Hydraulics Rep.* 1. UILU-ENG 87-5301, University of Illinois, Urbana, IL.

PAPOULIS, A. 1984 *Probability, Random Variables and Stochastic Theory*, 2nd Edn, McGraw-Hill.

PAYNE, F. R. & LUMLEY, J. L. 1967 Large eddy structure of the turbulent wake behind a circular cylinder. *Phys. Fluids* **10**, S194.

ROGALLO, R. S. 1981 Numerical experiments in homogeneous turbulence. *NASA TM* 81315.

ROGERS, M. M. & MOIN, P. 1987 The structure of the vorticity field in homogeneous turbulent flows, *J. Fluid Mech.* **176**, 33.

THEODORSEN, T. 1952 Mechanism of turbulence. In *Proc. 2nd Midwestern Conf. on Fluid Mech.* Ohio State University, Columbus, Ohio.

TUNG, A. T. C. 1982 Properties of conditional eddies in free shear flows. Ph.D. thesis, Dept. of Theor. and Appl. Mech., University of Illinois, Urbana, IL.

TUNG, T. C. & ADRIAN, R. J. 1980 Higher-order estimates of conditional eddies in isotropic turbulence. *Phys. Fluids* **23**, 1469.

TUNG, A. T. C., ADRIAN, R. J. & JONES, B. G. 1987 *Theor. and Appl. Mechanics Rep.* 483, UILU-ENG 87-6001, University of Illinois, Urbana, IL.

WILLMARTH, W. W. 1978 Survey of multiple sensor measurements and correlations in boundary layers. In *Coherent Structure of Turbulent Boundary Layers* (ed. C. R. Smith & D. E. Abbott), pp. 130–167. AFOSR/Lehigh University Workshop, Dept Mech. Engng & Mech., Bethlehem, PA.

WILLMARTH, W. W. & LU, S. S. 1972 Structure of the Reynolds stress near the wall. *J. Fluid Mech.* **55**, 65.